To the Graduate Council:

I am submitting herewith a thesis written by Thomas Levitte Cox entitled "Fiber Surface Roughness Characterization via Fourier Transformation of the Small-Angle Light Back Scattering Function". I have examined the final copy of this thesis for form and content and recommend that it be accepted in partial fulfillment of the requirements for the degree of Master of Science, with a major in Polymer Engineering.

John F. Fellers

John F. Fellers, Major Professor

We have read this thesis
and recommend its acceptance:

Roberto Benson

Paul Phillips

Accepted for the Council:

Associate Vice Chancellor
and Dean of The Graduate School

FIBER SURFACE ROUGHNESS CHARACTERIZATION
VIA
FOURIER TRANSFORMATION
OF THE
SMALL-ANGLE LIGHT BACK SCATTERING FUNCTION

A Thesis Presented for the
Master of Science
Degree
University of Tennessee, Knoxville

Thomas Levitte Cox

May 1992

ACKNOWLEDGEMENTS

I am very grateful to all the people that have supported and assisted me during my graduate work, in particular Dr. John F. Fellers for his patience, support, and guidance. In addition I would like to thank Dr. Lawrence J. Effler for the help and direction he has provided me. I would like to give a special thanks to Erette S. Bevins for his assistance with the fast Fourier transformation program, and to the members of my committee Dr. R.A. Benson and Dr. P.J. Phillips. A special thanks is also extended to Dr. R.R. Bresee for his assistance.

Above all I wish to extend thanks to the author's parents Mr. and Mrs. Tom E. Cox Jr. and his family for their support and prodding.

ABSTRACT

The experimental measurement of fiber surface roughness, by small-angle light back scattering coupled with Fourier transform analysis is presented. In addition the effects of scattering equipment parameters and fiber diameter, on the back scattering pattern, are investigated. A literature review on small-angle light scattering was performed to determine the extent of previous work in surface roughness determination. The review also provides the background information necessary to discuss the current research effort. A literature review was also conducted on the mathematical development of scattering theory for smooth and rough surfaces as well as the determination of surface roughness from scattering data using both optical and numerical methods for achieving Fourier transformations. The purpose of the research was to develop a method for accurately determining and quantitatively characterizing surface roughness, for comparing the surface roughness of different samples, and a method for graphically representing the surface topography.

TABLE OF CONTENTS

LIST OF FIGURES

LIST OF TABLES

I. INTRODUCTION

In the past much work has been done on the use of light scattering for the determination of surface roughness, with varying degrees of success. Although the exact details of the work have varied depending upon equipment configurations, wavelength of light, sample type, or assumptions used, generally the researchers arrived at the same conclusions. Mainly that light scattering, in principle, could be used to accurately determine the surface roughness of a sample [1-18]. Independent of the manner in which the data was treated, either optically or numerically, the results were similar. However, no researcher has reduced this idea into a completely satisfactory practical application. Also, several areas of research have been neglected by researchers. These areas include the determination of fiber surface roughness as well as the effects of fiber diameter and scattering equipment parameters on the back scattering pattern.

For the most part, previous work has centered on quality control and inspection of the surface finish of manufactured parts [7,8,10]. The purpose being to use light scattering for the measurement and characterization of the microtopography of rough surfaces [8]. The use of light scattering is desirable because it is non-contacting, sensitive, area sampling, and inherently absolute [11].

The idea that the surface roughness of a material might be measured by light scattering should be of interest to those who deal with the area of fiber science. This is because the surface roughness of a fiber affects the fiber's behavior during processing and its performance as a finished product. The fiber roughness is related to both the frictional and the optical properties. The frictional properties, in turn, affect the mechanical behavior of the fiber [12].

At the present time most light scattering methods for the determination of surface roughness, use some type of Fourier transform either optical or numerical [1-18]. This data is then represented in some form of intensity versus spatial frequency [12]. With this in mind, this paper presents a brief review of pertinent literature and proposes a mechanism for the determination of fiber surface roughness from Fourier transformed small-angle light back scattering data. The paper also presents the effects of fiber diameter and scattering equipment parameters on the scattering pattern.

II. REVIEW OF LITERATURE AND THEORY

2.1 INTRODUCTION

Within the past 30 years a great deal of work has been done in the area of light scattering from rough surfaces. Part of this work has involved the development of rigorous theory for scattering from rough surfaces [1,2,6,9,10,13,17]. Other researchers have work on the use light scattering to determine the roughness of a surface, usually by using the scattering data in correlation with some form of Fourier transform [1-18]. The transform having been achieved either optically [13-18] or mathematically [1-12].

Surface roughness 'is a measure of the topographic relief of a surface'.[19] Surface roughness is measured as height variations above or below the mean surface level and is usually expressed as a root-mean-square roughness value, this idea is illustrated in Figure 2.1. In this context the surface roughness of interest are those asperities which are of the order of magnitude to cause light scattering. These surface asperities are typically considered to be separated by submicrometers to fractions of a millimeter. The height of these asperities is generally considered to be from 0.1 micrometers (4 microinches) to 10 micrometers (400 microinches).[19]

The possibility that light scattering could be used for the

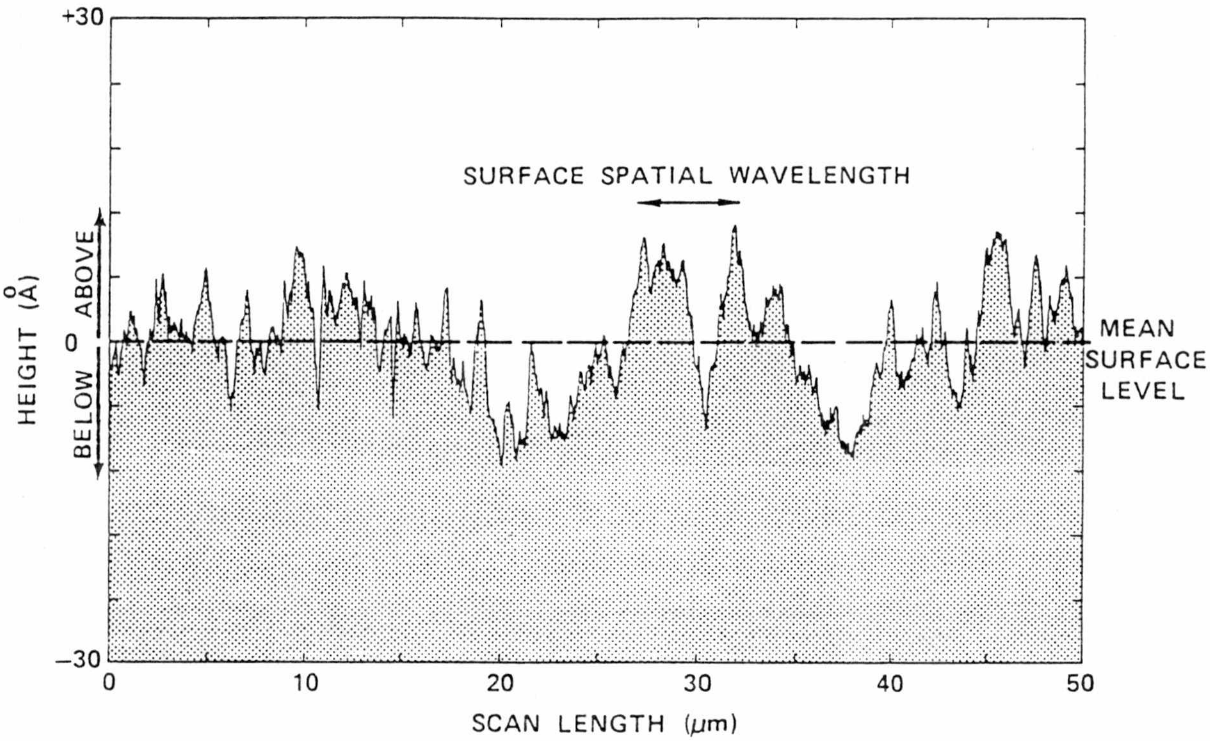

Figure 2.1 Schematic representation of a rough surface (Bennett and Mattsson)

determination of surface roughness can be understood by looking at how a beam of coherent, collimated, monochromatic light behaves when it strikes a conducting surface (Figure 2.2). If the surface is perfectly smooth, 'all the reflected light remains in a collimated beam, known as the specular beam, propagating in a direction given by Snell's law and having essentially the same angular divergence properties as the incident beam'[7]. If however, the incident beam strikes a rough surface (Figure 2.3) the light will be scattered in a distribution of angles. 'The intensity and pattern of the scattered light depends on the amplitude and wavelengths of the surface topography, the material properties of the surface, and the wavelength of the incident light.'[7[This scattering, from rough surfaces, can be 'viewed as scattering from sets of sinusoidal surface components with different amplitudes, wavelengths, and directions across the surface resulting from a two-dimensional Fourier decomposition of the function describing the surface topography' [7].

2.2 RIGOROUS SCATTERING THEORY

In the late 1950's Bennett and Porteus worked on the relationship between surface roughness and specular reflectance. As a result they derived an expression for the total integrated scattering based on equations they developed for the specular reflectance and the non-specular scattering from a rough surface. In addition they developed a relationship between the root mean squared slope and the autocovariance length for a flat surface [1]. Bennett and Porteus described the

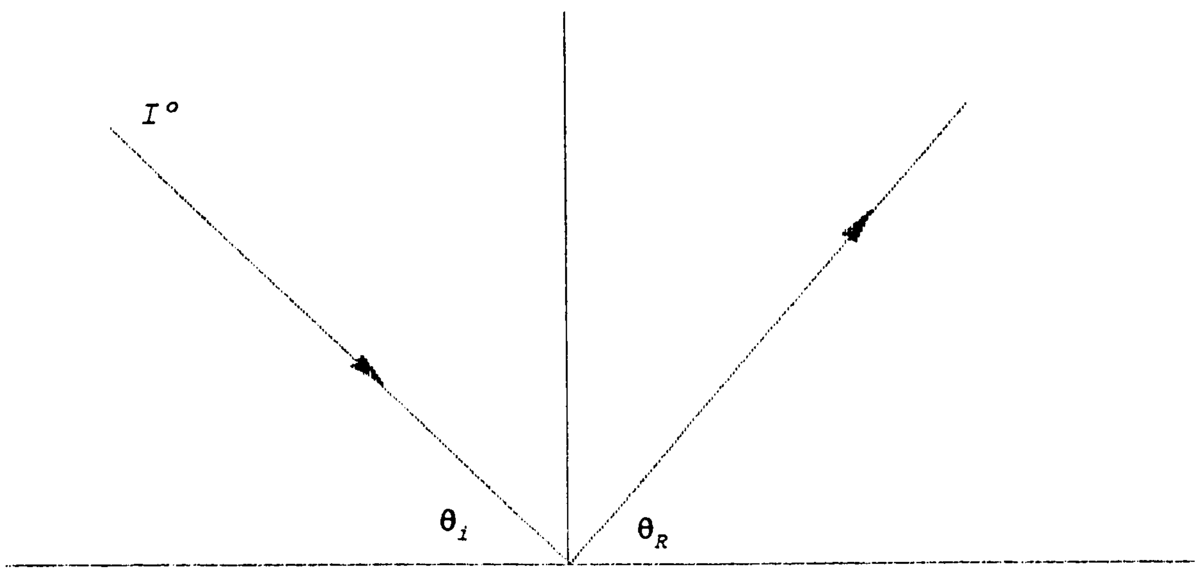

Figure 2.2 Schematic of the Scattering Geometry from a Smooth Surface

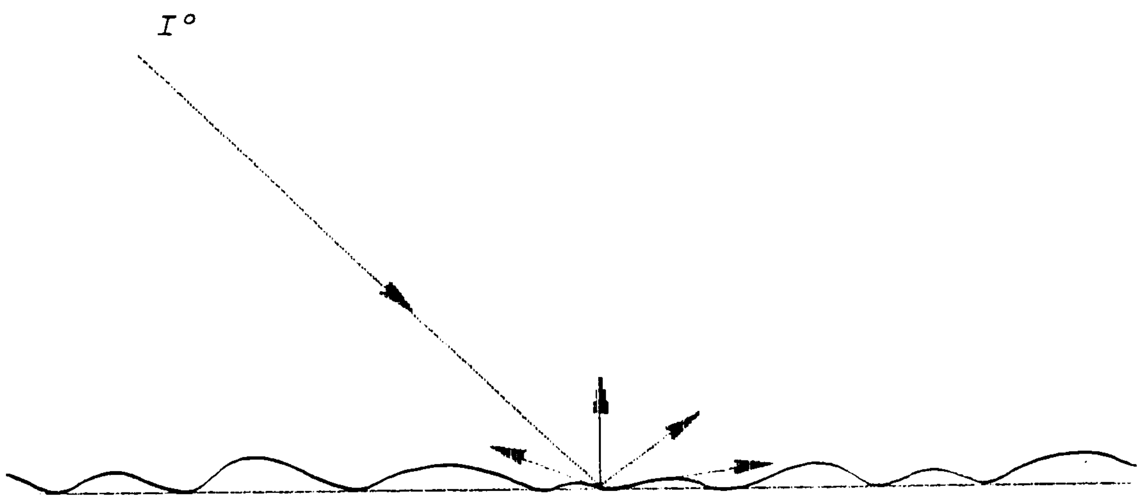

Figure 2.3 Schematic of the Scattering Geometry from an Arbitrarily Rough Surface

specular reflectance as:

$$R_s = R_0 \exp[-(4\pi\sigma)^2/\lambda^2] \tag{2-1}$$

where R_s is the specular reflectance of a rough surface at normal incidence, R_o the reflectance of a perfectly smooth surface, σ the root mean square roughness, defined as the root mean square deviation of the surface from the mean surface level, and λ the wavelength of incident light. Note that R_s is a function of the specular reflectance from a theoretical smooth surface multiplied by a 'roughness factor'. This factor ranges from 1, for a smooth surface, and decreases to zero as the roughness increases. The angular dependence of the diffusely scattered light, the non-specular scattering, can be described by:

$$r_d(\theta)\,d\theta =$$

$$R_0 2\pi^4 (a/\lambda)^2 (\cos\theta+1)^4 \sin\theta \, \exp[-(\pi a \sin\theta)^2/\lambda^2]\, d\theta \tag{2-2}$$

where a is the autocovariance length. If the roughness has a Gaussian distribution it can be shown that the autocovariance length (a) is related to the root mean square slope (m) of the profile of the surface by:

$$a = 1.41\sigma/m \tag{2-3}$$

Therefore, at normal reflectance, the contribution from diffuse scattering is:

$$\int_0^{\Delta\theta} I_d(\theta)\,d\theta = R_0 \frac{2^5\pi^4}{m^2} (\sigma/\lambda)^4 (\Delta\sigma)^2 \qquad (2\text{-}4)$$

Here again, notice that the diffuse scattering is a function of the specular reflectance from a theoretical smooth surface multiplied by a 'roughness factor', with this factor increasing as roughness increases. The total integrated reflectance would then be a summation of the specular reflectance and the non-specular scattering, or diffuse scattering, from the surface and can be described by:

$$R = R_0 \exp[-(4\pi\theta)^2/\lambda^2] + R_0 \frac{2^5\pi^4}{m^2} (\theta/\lambda)^4 (\Delta\theta)^2 \qquad (2\text{-}5)$$

It should be noted that equation 2-5 reduces to equation 2-1 at long wavelengths, i.e. the surface appears smooth. [1]

Beckmann, in his work, described the mean square amplitude for back scattering. Beckmann's work dealt with the scattering from random surfaces. Using the coordinate system defined by Figure 2.4, the mean square amplitude for back scattering can be defined as:

$$\langle EE^* \rangle = \frac{E_0^2 \lambda^2}{8\pi A \cos^4\theta \sum_j s_j^2} \exp\left(-\frac{\tan^2\theta}{2\sum_j s_j^2} \right) \qquad (2\text{-}6)$$

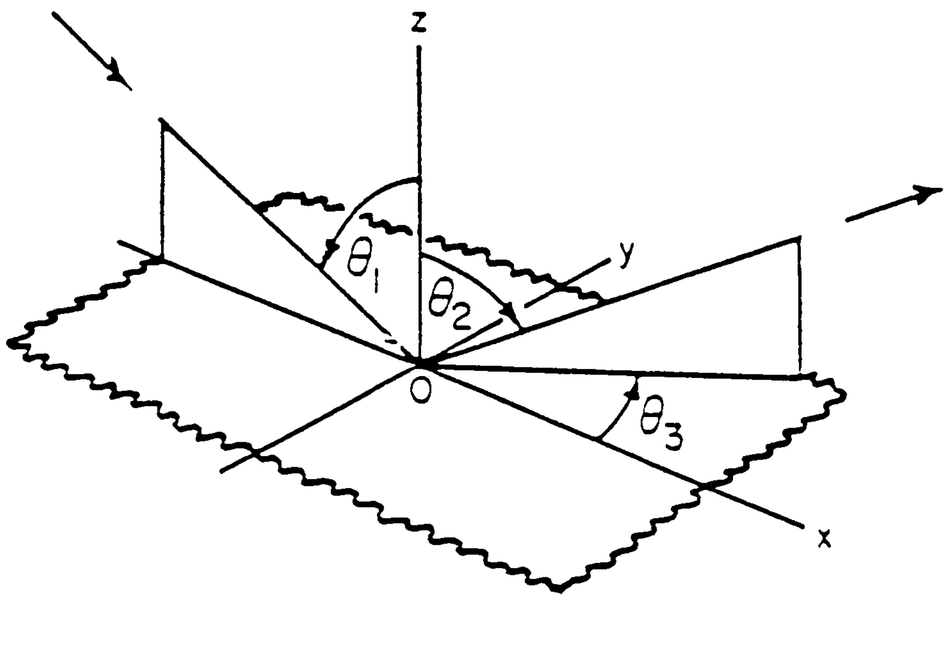

Figure 2.4 Scattering Geometry (Beckmann)

where $<EE^*>$ is the mean square amplitude scattered, $E_o = kA / \pi R_o$ and is the amplitude of the field strength reflected by a plane surface, $k = 2\pi / \lambda$, A is the area illuminated, R_o the distance, λ the wavelength of incident radiation, and s_j the root mean square slope of the surface roughness components. Note that this equation like that of Bennett and Porteus relates the diffuse scatter to the specular reflection from a theoretical smooth surface modified by a factor that causes the function to decrease as roughness increases. However, Beckmann suggested that his equations were accurate for only slightly rough surfaces [2].

2.3 FOURIER OPTICS AND FOURIER TRANSFORMS

A Fourier transformation can be described as 'a linear transformation which produces a useful mathematical relation between a waveform and the phase amplitude density of its frequency content'[20]. The transform does so by resolving a waveform into its sinusoidal components. 'The Fourier transform, X(f), of a complex and single-valued function x(t) is defined mathematically as:

$$X(f) = \int_{-\infty}^{\infty} x(t) \exp(-j2\pi f t)\, dt \qquad (2\text{-}7)$$

where t and f are real variables, and j is the imaginary unit.'[21] If t is time in seconds then f would be frequency in Hertz. The inverse

Fourier transform of X(f) is defined mathematically as:

$$x(t)=\int_{-\infty}^{\infty} X(f)\exp(j2\pi ft)\,df \tag{2-8}$$

The Fourier transform property of a lens can be established using the diffraction integral describing the propagation of monochromatic light in free space [21]. The diffraction integral can be used to mathematically describe all the optical phenomena related to Fourier optics. The integral can be derived from Fourier transform considerations coupled with the ideas of plane waves and complex amplitudes.

A better understanding of the ability of a converging lens to perform a two-dimensional Fourier transformation can be obtained from reviewing the various Fourier transformation configurations. In the following three configurations 'the illumination is assumed to be monochromatic and the distribution of the light amplitude across the back focal plane of the lens is of concern'[22]. Figure 2.5 illustrates the three configurations reviewed. In 2.5 (a) 'the object to be transformed is placed directly against the lens'[22]. In 2.5 (b) 'the object is placed at a distance d in front of the lens'[22]. In case 2.5 (c) 'the object is placed behind the lens at a distance d from the focal plane'[22].

Consider the situation in Figure 2.5 (a), where the object is placed against the lens. Let the object having an amplitude transmittance of t(x,y), be placed in front of and against a converging lens of focal

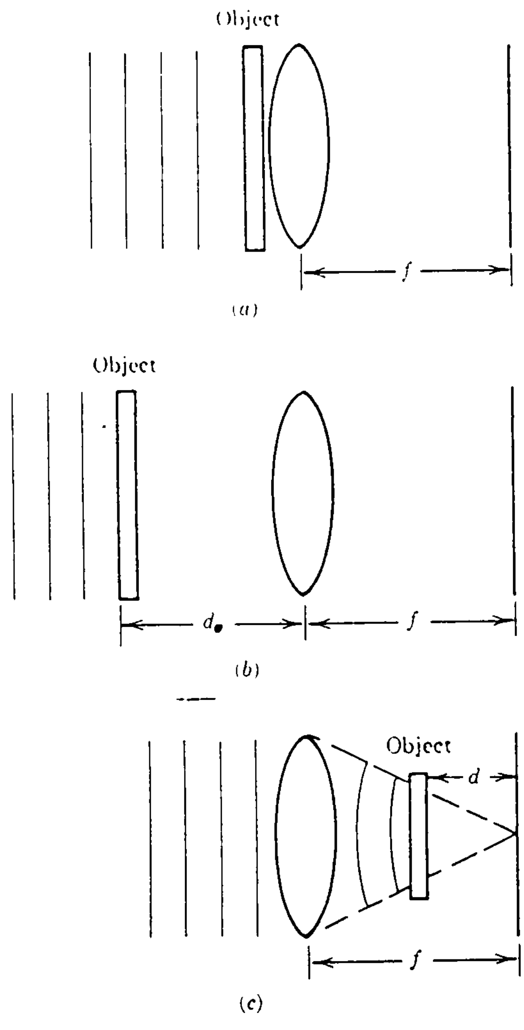

Figure 2.5 Fourier Transforming Configurations (Goodman)
(a) Object placed against the lens
(b) Object placed in front of lens
(c) Object placed behind lens

length f. If the object is normal to an incident beam of monochromatic light of amplitude A the disturbance on the lens is

$$U_1(x,y) = At(x,y) \tag{2-9}$$

let the pupil function P(x,y) account for the lens aperture, where P(x,y) is defined by

$$P(x,y) = \begin{cases} 1 & \text{inside the lens aperture} \\ 0 & \text{otherwise} \end{cases} \tag{2-10}$$

The amplitude distribution behind the lens becomes

$$U_1'(x,y) = U_1(x,y)\,P(x,y)\exp[-j(k/2f)\,(x^2+y^2)] \tag{2-11}$$

Where f is the focal length and k is $2\,\pi\,/\,\lambda$. Applying the Fresnel diffraction formula, putting z = f, and simplifying the equation becomes;

$$U_f(x_f,y_f) = \frac{\exp[j(k/2f)\,(x_f^2+y_f^2)]}{j\lambda f}$$

$$X\iint_{-\infty}^{\infty} U_1(x,y)\,P(x,y)\;\exp[-j(2\pi/\lambda f)\,(xx_f+yy_f)]\,dxdy \tag{2-12}$$

Thus the field distribution U_f is proportional to the two-dimensional Fourier transform of the incident field subtended by the lens aperture.

If it is assumed that the object is smaller than the lens aperture, P(x,y) can be neglected leaving.

$$U_f(x_f, y_f) = A\frac{\exp[j(k/2f)(x_f^2+y_f^2)]}{j\lambda f}$$

$$X\iint_{-\infty}^{\infty} \exp[-j(2\pi/\lambda f)(xx_f+yy_f)]\,dxdy \quad (2\text{-}13)$$

Measurement of the intensity distribution across the focal plane yields the power spectrum of the object;

$$I_f(x_f, y_f) =$$

$$A^2/\lambda^2 f^2 \left|\iint_{-\infty}^{\infty} t(x,y)\exp[-j(2\pi/\lambda f)(xx_f+yy_f)]\,dxdy\right|^2 \quad (2\text{-}14)$$

Now consider the situation in Figure 2.5 (b). The object is placed in front of the lens and is located a distance d from the lens, then let $F(f_x,f_y)$ represent the Fourier spectrum of the light transmitted by the object, and $F_1(f_x,f_y)$ be the Fourier Spectrum of the light incident on the lens. Assuming Fresnel approximations are valid the equation is

$$F_1(f_x, f_y) = F(f_x, f_y)\exp[-j\pi\lambda d(f_x^2+f_y^2)] \quad (2\text{-}15)$$

Neglecting the finite extent of the lens aperture (P = 1) and substituting into equation 2.13 we have

$$U_f(x_f, y_f) =$$

$$\frac{\exp[j(k/2f)(1-\frac{d}{f})(x^2+y^2)]}{j\lambda f} F(x_f/\lambda f, y_f/\lambda f) \qquad (2\text{-}16)$$

or the equation corresponding to 2.13

$$U_f(x_f, y_f) = A\frac{\exp[j(k/2f)(1-\frac{d}{f})(x_f^2+y_f^2)]}{j\lambda f}$$

$$X \iint_{-\infty}^{\infty} t(x,y)\exp[-j(2\pi/\lambda f)(xx_f+yy_f)]\,dxdy \quad (2\text{-}17)$$

'Thus the amplitude and phase of the light at coordinates (x_f, y_f) are again related to the amplitude and phase of the object spectrum at frequencies $(x_f/\Pi f, y_f/\Pi f)$.'[22] Notice that a phase factor precedes the transform integral but vanishes at d = f.

Finally, let the object be placed behind the lens, as in 2.5 (c). The object has a transmittance of t and is located a distance d from the focal plane of the lens. 'Let the lens be illuminated by a normal incident plane wave of amplitude A. Then incident on the object is a spherical wave converging toward the back focal point of the lens.'[22]

Using the geometrical-optics approximation the amplitude of the wave impinging on the object is Af/d. If the lens has a diameter of D_L, the diameter of the circular region illuminated is $D_L d/f$, and the pupil function is P[x(f/d),y(f/d)]. Using the paraxial approximation to the spherical wave we may write

$$U(x,y) =$$

$$\left(\frac{Af}{d} P(x(f,d),y(f,d)) \exp[-j(k/2d)(x^2+y^2)]\right) t(x,y) \quad \text{(2-18)}$$

again, assuming Fresnel diffraction is valid it can be shown that

$$U_f(x_f,y_f) = A\frac{\exp[j(k/2d)(x_f^2+y_f^2)]}{j\lambda f}(f/d) \iint_{-\infty}^{\infty} t(x,y)$$

$$P(x(f,d),y(f,d)) \exp[-j(2\pi/\lambda d)(xx_f+yy_f)]\, dxdy \quad \text{(2-19)}$$

Thus the focal-plane amplitude distribution is the Fourier transform of the portion of the object subtended by the projected lens aperture [22]. Note that examination of equations 2-13, 2-17, and 2-19 will show that the relationship between the Fourier transform of the object and the focal plane is not an exact one. They are related by the amplitude, incident wavelength, and focal length.

2.3.1 REVIEW OF FOURIER OPTICS FOR THE ANALYSIS OF SURFACE ROUGHNESS

As has been stated, two paths have been taken in an attempt to make use of light scattering data for the purpose of surface roughness determination. One path taken was numerical transforms and the other optical transforms. The researchers approaching the problem using optical methods have relied on lens arrangements similar to those illustrated in Figure 2.6. These researchers took note of the fact that a converging lens has the property of performing a two-dimensional Fourier transformation [13-18].

One such researcher, R.A. Sprague, set out to examine the applicability of an optical method and 'experimentally verify a simple physical theory relating speckle contrast in broadband illumination to surface roughness'[13]. Sprague used a set of samples that contained 'a range of roughness values produced with a variety of finishing techniques'[13]. Although no conclusive results were obtained, it was noted that the data did show a good relation between speckle contrast and root-mean-square surface roughness in the range of roughnesses between 0.2 μm and 3.2 μm. It was also demonstrated that the measured roughness was independent of surface finish [13]. Meaning that whether the sample had a dull or glossy finish the measured roughness would be the same.

Several years after Sprague's work B.J. Pernick set out 'to develop a tool for surface quality inspection of machined metal specimens employing a coherent optical processing system'[14]. Pernick, referring

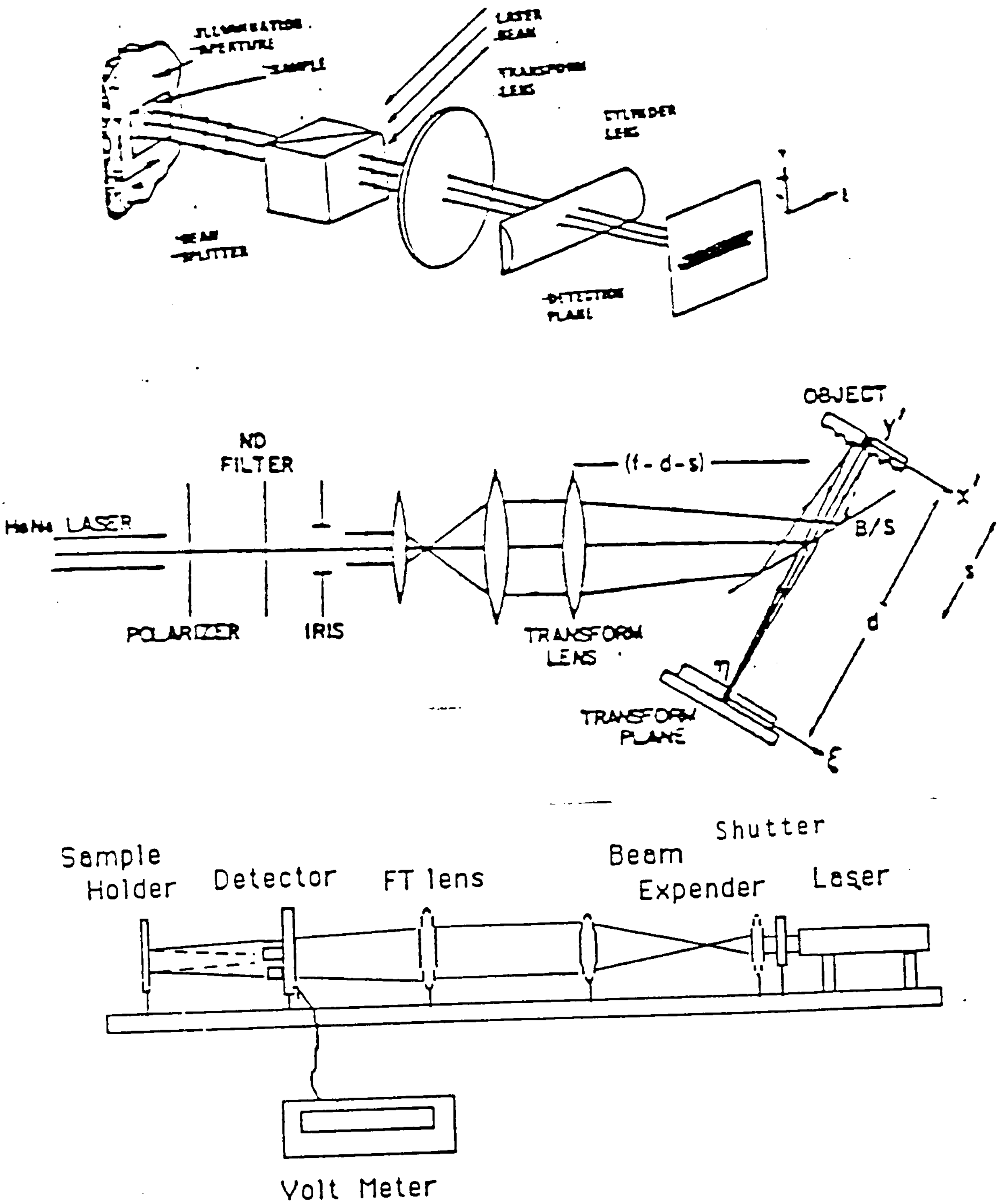

Figure 2.6 Methods for Achieving Optical Fourier Transforms

to the work of others, demonstrated that the patterns obtained by an 'optical Fourier transform distribution of laser-illuminated samples were related to roughness levels for machined metal surfaces'[14]. He further asserted that this evidence could serve as the basis for a practical instrument. Pernick used a surface roughness scale and microfinish comparator for his samples. The comparator used was an industry standard. The results obtained 'demonstrated that the relationship between a far-field scattered light signature and integrated Gaussian curve parameters can be used to measure surface roughness for metal samples'[14]. Pernick asserted that an optical Fourier system could be developed for the purpose of surface roughness measurement [14].

At approximately the same time that Pernick was researching the possibility of designing an instrument for surface roughness determination. E.G. Thwaite was trying to 'determine the limitations of the optical Fourier transform technique in directly determining the power spectrum of opaque objects'[16]. He noted that the determination of the power spectrum would provide a practical tool for the determination of the topographical properties of surfaces. Thwaite noted that the success of the optical method is dependent upon 'being able to resolve the structure of the image in the Fourier plane' and upon 'how well the light distribution across the object represents its amplitude features'[16]. Use was made of the Wiener-Khintchine theorem that states that the angular power spectrum is obtained from the Fourier transformation of the autocorrelation function.[16] Thwaite noted that the converging lens setup would perform the Fourier transformation. Through his studies

Thwaite showed that the power spectrum, obtained by optical Fourier transformation, could be directly interpreted [16].

In work done by T. Horiuchi, et al. an optical method for the measurement of surface roughness, 'independent of correlation length and reflectance variation caused by contamination of the surface' is described. Horiuchi defines a ratio as being a normalized maximum speckle intensity dependent only on the roughness of the sample and not on the reflectance.

$$\alpha = I_m / I_0 \tag{2-20}$$

where I_m is the maximum intensity of speckles and I_0 is the total power of the scattered light. Horiuchi, et al. concluded that the surface roughness could be measured with the speckle pattern assuming that the following conditions were fulfilled '(1) the speckle intensity maximum is well detected and (2) the ratio α of the maximum intensity to the total power of the scatted light is used as the scale of roughness measurement' [18].

2.3.2 REVIEW OF FOURIER TRANSFORMS FOR THE ANALYSIS OF SURFACE ROUGHNESS

While some researchers worked on obtaining a Fourier transform optically others have approached the problem by using a numerical Fourier transform on scattering data [4-12]. One researcher, P.J. Chandley, working under the assumption of a 'Gaussian first order probability density function of height, studied the autocorrelation function of height by means of the Fourier transform of the ensemble average far-field scattered light' [4]. Chandley used ground glass surfaces, the results indicating that the normalized autocovariance function of height on a rough surface could be determined from the Fourier transform of the ensemble far-field scattered light intensity. He defined the normalized autocovariance function of height on a rough surface as

$$C(p) = \frac{1+\log_e\left(\frac{C_v(p)}{C_v(0)}\,(1-\exp(-\sigma^2)+\exp(-\sigma^2)\right)}{\sigma^2} \qquad (2\text{-}21)$$

where C(p) is the autocovariance function, $C_v(p)$ is the Hankel transform of the autocovariance function, Cv(0) is the autocovariance function of a smooth surface, and σ is the square root of the variance height. However, the method is not valid for very rough surfaces. Chandley found that when the height of the scatteres was of the same order as the incident light, or larger, the method used was not accurate. [4]

Later, in an attempt to further develop his work, Chandley looked at the assumption of a Gaussian form for the autocorrelation function of surface height. He found that the assumption, of Gaussian form, was not valid. However, he found that measurements of the variance of ground glass surfaces were in agreement for different scattering geometries between light scattering and optical methods [5].

O.M. Mendez, et al. later looked at how a Fourier transformed model would behave as a function of asperity depth. They found that for shallow asperities the Fourier transform worked well but there was an increasing inaccuracy with increasing depth of asperity [8].

However, none of these studies looked at the problem of fibers. Later, Cheng Lou [12] looked at the determination of fiber roughness using light back scattering and Fourier transforms. In this study the discrete Fourier transform pair used was;

$$F(u,v) = \frac{1}{MN}\sum_{x=0}^{M-1}\sum_{y=0}^{N-1} f(x,y)\exp\left[-j2\pi\left(\frac{ux}{M}+\frac{vy}{N}\right)\right] \qquad (2\text{-}22)$$

and

$$f(x,y) = \sum_{u=0}^{M-1}\sum_{v=0}^{N-1} F(u,v)\exp\left[j2\pi\left(\frac{ux}{M}+\frac{vy}{N}\right)\right] \qquad (2\text{-}24)$$

where M is the maximum number of x points and N is the maximum number of y points. However, a fast Fourier transform (FFT) was used to approximate the above equations in an effort to reduce computation time. These equations give a triaxial representation shown in Figure 2.7. The FFT was

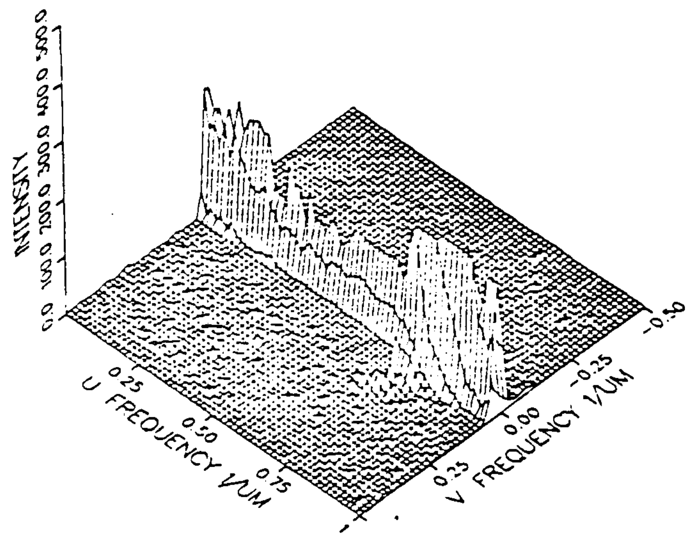

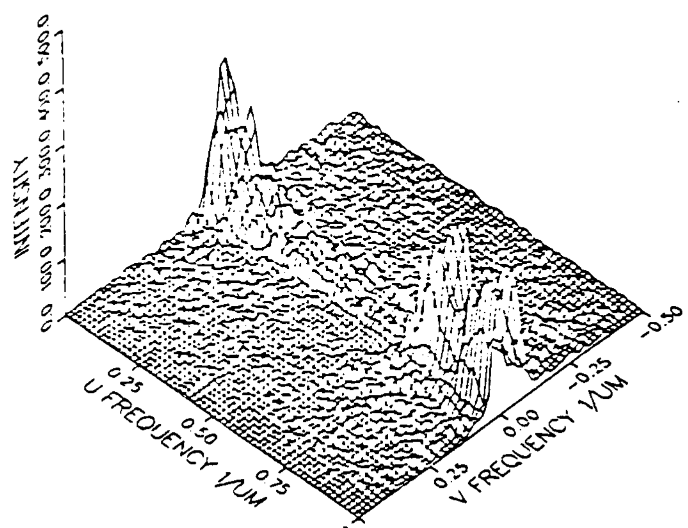

Figure 2.7 3-Dimensional Representation of Surface Topography Obtained by Fourier Transformation Analysis (Cheng)

performed as a FORTRAN subroutine. Cheng used this model to investigate several fibers of different surface roughness (nylon, polypropylene, rayon, cotton, and wool). It was found that the model suggested increasing surface roughnesses as would be expected. The subroutine also defined a parameter called the roughness coefficient (RC) defined as

$$RC=\frac{I_t}{I_0} \tag{2-24}$$

Where I_o is the intensity at zero frequency and I_t is the total intensities scattered at other frequencies. The I_t term will be zero for a perfectly smooth surface. Note that this is similar to the α value used by Horiuchi, et al. [7] for the optical Fourier transform. This RC also showed a strong dependence on the surface roughness for the samples used [5].

2.4 Methods for Determining Surface Roughness

Current methods for the determination of the surface roughness of samples are either contacting or optical. Contacting instruments use a diamond stylus. In contacting methods the diamond stylus is drawn across the surface of a sample. The movements of the stylus are converted to electrical signals, which are amplified and can be recorded on chart paper.[19] Although stylus instruments are considered to be very accurate they have a 'number of serious disadvantages: they are relatively expensive, they are sensitive to ambient vibrations particularly on smoother surfaces, they are relatively slow to set up and use, particularly on workpieces of curved section, and the stylus, being diamond, generally marks the workpiece and because of its finite size may miss very small irregularities'[15]. In addition, the stylus may be affected by dirt, oil, or films on the surface of the sample.[19]

Most common noncontacting profilers use a combination of light beams and some form of microscope. The standard methods use an interferometer. Interferometers use either the test surface or a separate surface as a reference. 'Several instruments are based of the principle of the differential interference contrast microscope and measure height differences (slopes) between two closely spaced points separated by approximately 1 micrometer and then integrate detector signals to obtain a surface profile.'[19] However, in addition to being expensive, many optical profilers use probe beams of less than 10 micrometers in diameter. This small beam make the sampling of large surface areas difficult.

III. COMPUTER SIMULATION STUDIES

3.1 INTRODUCTION

In order to accomplish the goals proposed for this work, it was necessary to rely heavily upon computer assistance. As a result use was made of several commercially available software packages. In addition to these, four specialized computer programs had to be developed by the author.

Included in the commercial software was Tecmar's Video Van Gogh package and 3-D Visions Corp's GraphTool plotting package. The Video Van Gogh package was used to digitize, store, and retrieve the scattering pattern. The package digitizes the pattern using a 64K grid composed of 249 x 236 pixel locations. The pixel locations range from 2,16 in the upper left corner to 250,251 in the lower right corner. The intensity of each pixel location is recorded as a relative intensity value ranging from 0 to 255. A value of 0 represents pure black, or no detected light intensity, and a value of 255 represents pure white, or the maximum light intensity that can be detected by the camera. The value of the intensity is dependent on the gain and contrast setting of the camera, the f-stop of the lens, and the camera-to-screen distance. [23] After the data was digitized, GraphTool software was used to generate three-dimensional representations of the Fourier transformed images as well as X,Y coordinate plots.

As stated before, it was necessary to develop additional programs to assist in interpreting the data. To this extent, four programs were developed. One program produces the theoretical scattering pattern of an infinitely smooth fiber. A second similar program produces the theoretical scattering from an infinitely smooth flat surface. Another performs a numerical Fast Fourier transform on the theoretical data as well as data gathered in the laboratory. A final program was needed to perform the actual calculation of the surface roughness from the data. The theoretical data, for an infinitely smooth fiber, as well as the infinitely smooth flat surface, were necessary for the determination of the specular region of a small-angle back scattering pattern. The Fourier transform was necessary to determine the surface topography from a small-angle back scattering pattern. A full listing of all user generated programs is presented in Appendices A through D.

3.2 SMOOTH FIBER SURFACE COMPUTER GENERATED SCATTERING

As stated before the scattering from an infinitely smooth flat surface can be described by Snell's Law. When the smooth surface is a fiber the scattering can also be described by Snell's Law if allowances are made for the cylindrical geometry. Take for example, the fiber illustrated in Figure 3.1, of length L with a diameter D_f. The fiber is completely bathed by an incident beam of diameter D_b. Assume that the fiber axis is perpendicular to the incident beam. Under these conditions the scattering from the fiber can be described by looking at a

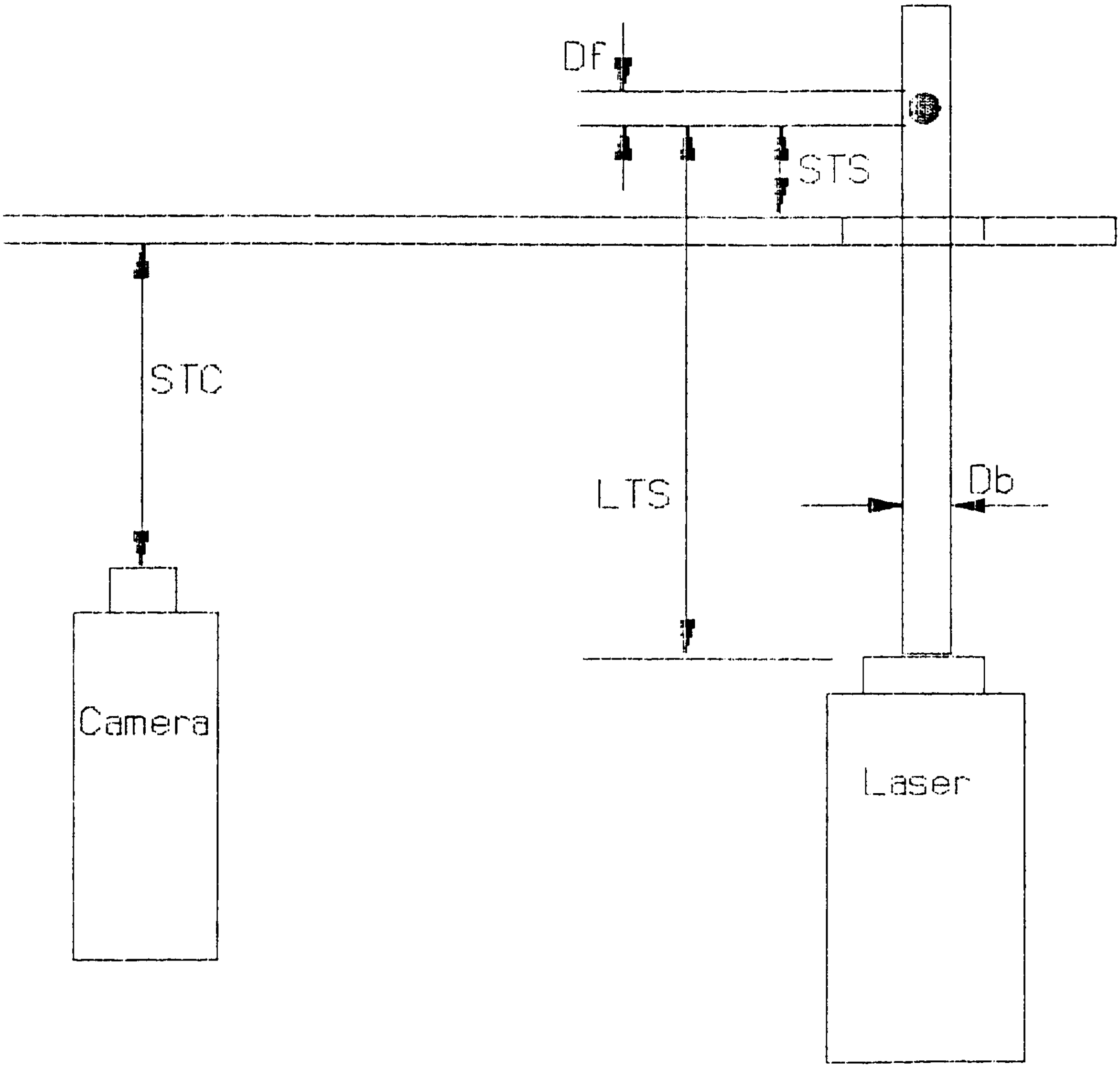

Figure 3.1 Schematic Diagram of Sample Fiber to Incident Beam Geometry

single quadrant representing all incident angles between 0° and 90° (Figure 3.2). As a result of this, the fiber diameter is not important, all that is needed is the refractive index (n) and the Sample-to-Screen distance. Using Snell's Law:

$$Sin\theta_i = n\, Sin\theta_r \qquad (3\text{-}1)$$

Where θ_i is the incident angle, θ_r is the reflected angle, and n is the refractive index. Therefore the Sample-to-Screen distance, the distance the scattered light travels, can be determined using Figure 3.3.

$$d = \frac{STS}{Cos(180 - \theta_i - \theta_r)} \qquad (3\text{-}2)$$

Where d is the distance traveled by scattered light, and STS is the Sample-to-Screen distance. Knowing the distance traveled by the scattered light the inverse square law can be used to determine the intensity of the light on the imaging screen by

$$I = \frac{\alpha I_0}{d^2} \qquad (3\text{-}3)$$

Where I is the intensity on the imaging screen, α is the absorbtivity of fiber, and I_o is the incident intensity. To incorporate these ideas into the Video Van Gogh software three additional steps are needed. First,

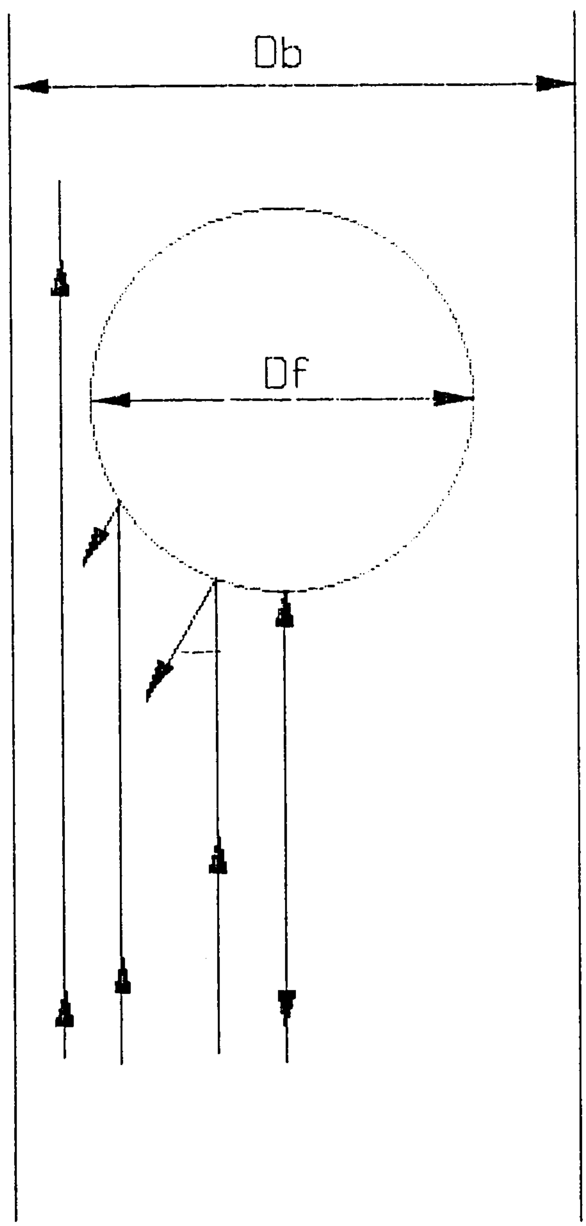

Figure 3.2 Fiber Cross-Sectional Scattering Geometry.

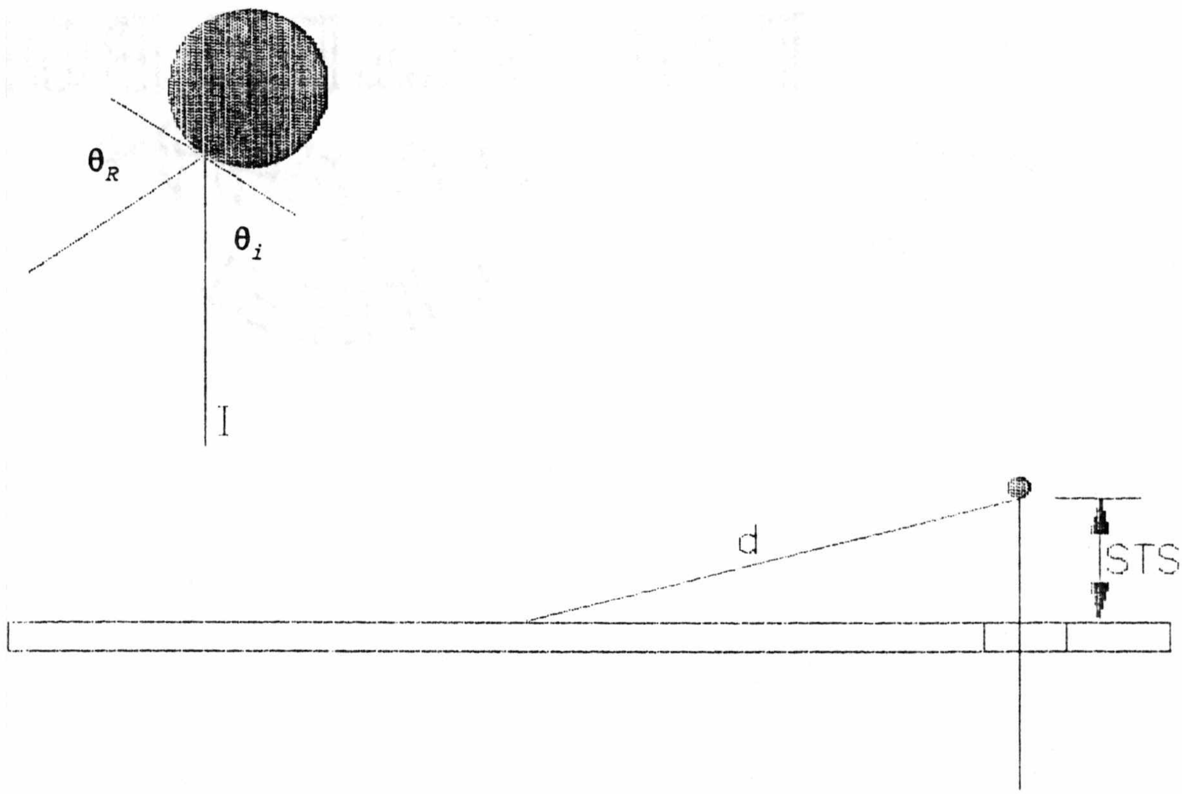

Figure 3.3 Determination of Path Traveled by Scattered Light

there needs to be an intensity value calculated for each pixel location recognized by the Video Van Gogh software. By knowing the camera-to-screen distance the number of pixel locations per centimeter can be obtained by the following equations [23]

$$X=\frac{712.6}{CTS^{1.05}} \tag{3-4}$$

$$Y=\frac{905.9}{CTS^{1.04}} \tag{3-5}$$

Knowing the number of pixels it is possible to back calculate using equation 3-2 and obtain the incident angles giving the intensities for the first and last pixel locations. Knowing the number of pixels and the starting and ending incident angle, the step size for the incident angle can be readily obtained. After a value has been obtained for each pixel the intensity value needs to be normalized, therefore, each intensity value is divided by the largest intensity value calculated. This gives normalized intensities between 0 and 1. The final step performed is to assign a gray level for each pixel based on the normalized intensity value. This can be accomplished by multiplying the normalized intensity by 255, the gray levels recognized by Video Van Gogh. This process puts the theoretical scattering data in terms of the Video Van Gogh system. These procedures are accomplished by the user written BASICA program TSTREAK.BAS.

The scattering from a flat smooth surface can be described directly by Snell's Law. The specular scattering from a flat smooth surface will be represented as a dot, for a sample placed perpendicular to the incident beam. If this is the case the specular scattering is reflected back into the incident beam and can not be used in calculations. However, if the sample is placed at an off angle the specular scattering is reflected out of the incident beam and can be recorded and used in calculations. This rotation shifts the specular dot into an ellipse, as shown in Figure 3.4. For ease in calculation the specular ellipse is approximated by a rectangle. The development of the theoretical scattering then becomes analogous to the one presented for a fiber. Noting that the angle of incidence is a constant the distance the scattered light travels is readily determined. The theoretical scattering is preformed by the BASICA program TDOT.BAS.

3.3 COMPUTER PERFORMED MATHEMATICAL FOURIER TRANSFORM

The Fourier transform computations are based on work previously performed by Cheng Lou in his master's work at the University of Tennessee. The transform uses the discrete Fourier pair defined as

$$F(u,v) = \frac{1}{MN}\sum_{x=0}^{M-1}\sum_{y=0}^{N-1} f(x,y)\exp\left[-j2\pi\left(\frac{ux}{M}+\frac{vy}{N}\right)\right] \qquad (3\text{-}6)$$

for u = 0,1,2,...,M-1, v = 0,1,2,...,N-1

and

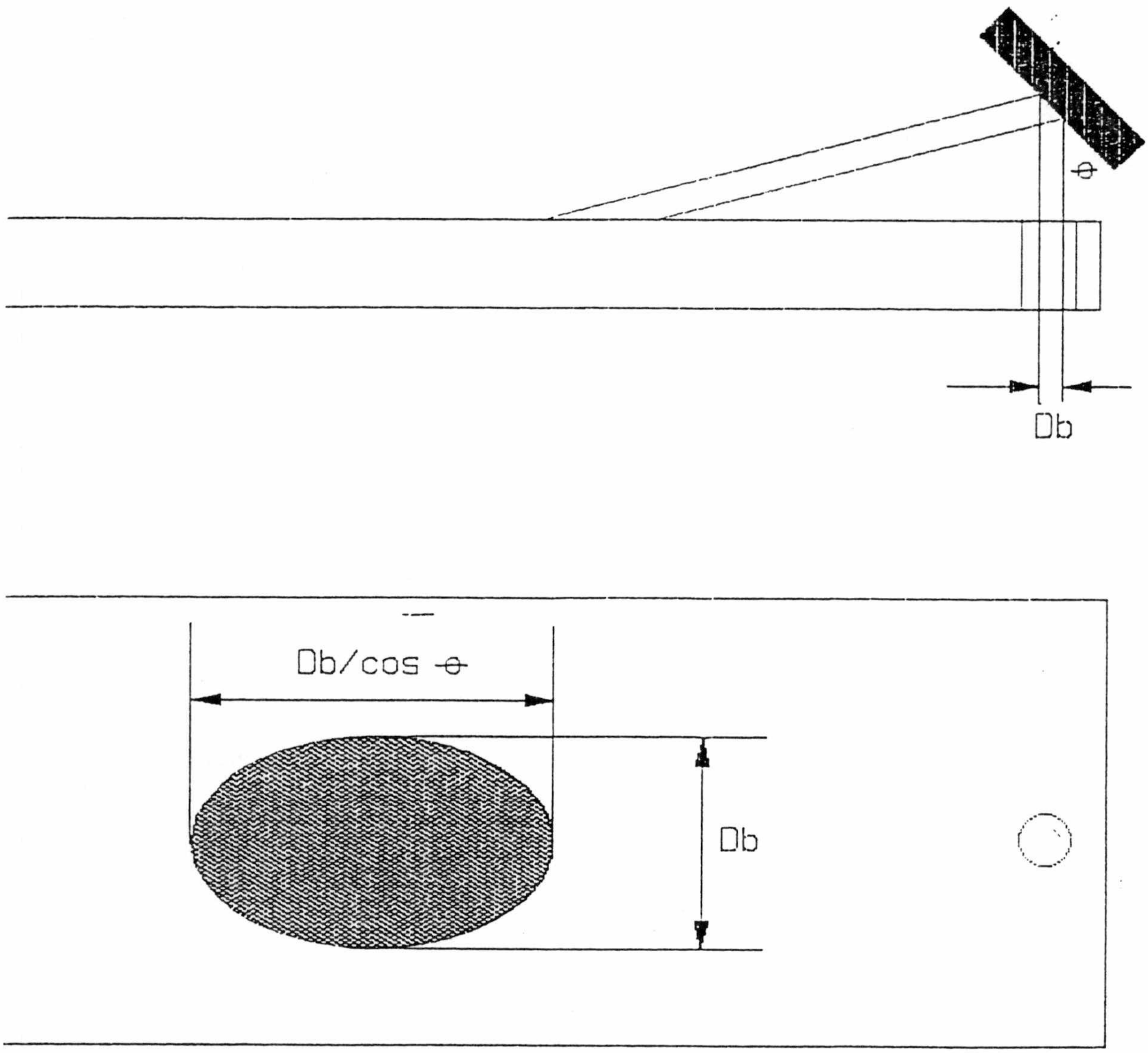

Figure 3.4 Schematic Diagram of Flat Sample to Incident Beam Geometry

$$f(x,y) = \sum_{u=0}^{M-1} \sum_{v=0}^{N-1} F(u,v) \exp\left[j2\pi\left(\frac{ux}{M} + \frac{vy}{N}\right)\right] \tag{3-7}$$

for x = 0,1,2,...,M-1, y = 0,1,2,...,N-1

where M is the maximum number of x points and N is the maximum number of y points. In an effort to save computational time a Fast Fourier transformation program was developed by E.S. Bevins. The program performed the Fourier transformation using the theory of separability. The transform is performed using the following.

$$F(u,v) = \frac{1}{N}\sum_{x=0}^{N-1} \exp\left(-j2\pi\frac{ux}{N}\right)\sum_{y=0}^{N-1} f(x,y) \exp\left(-j2\pi\frac{vy}{N}\right) \tag{3-8}$$

3.4 COMPUTER PERFORMED SURFACE ROUGHNESS CALCULATION

The calculation of the surface roughness coefficient is based on the ratio of the specular reflection from an actual fiber to the theoretical specular reflection from the same fiber, if perfectly smooth and under the same conditions. The rationale for this procedure can be understood by examining Figure 3.5, noting that as the roughness increases the intensity curve of the specular region shifts. When light strikes a perfectly smooth fiber all the light is reflected as the specular streak. However,

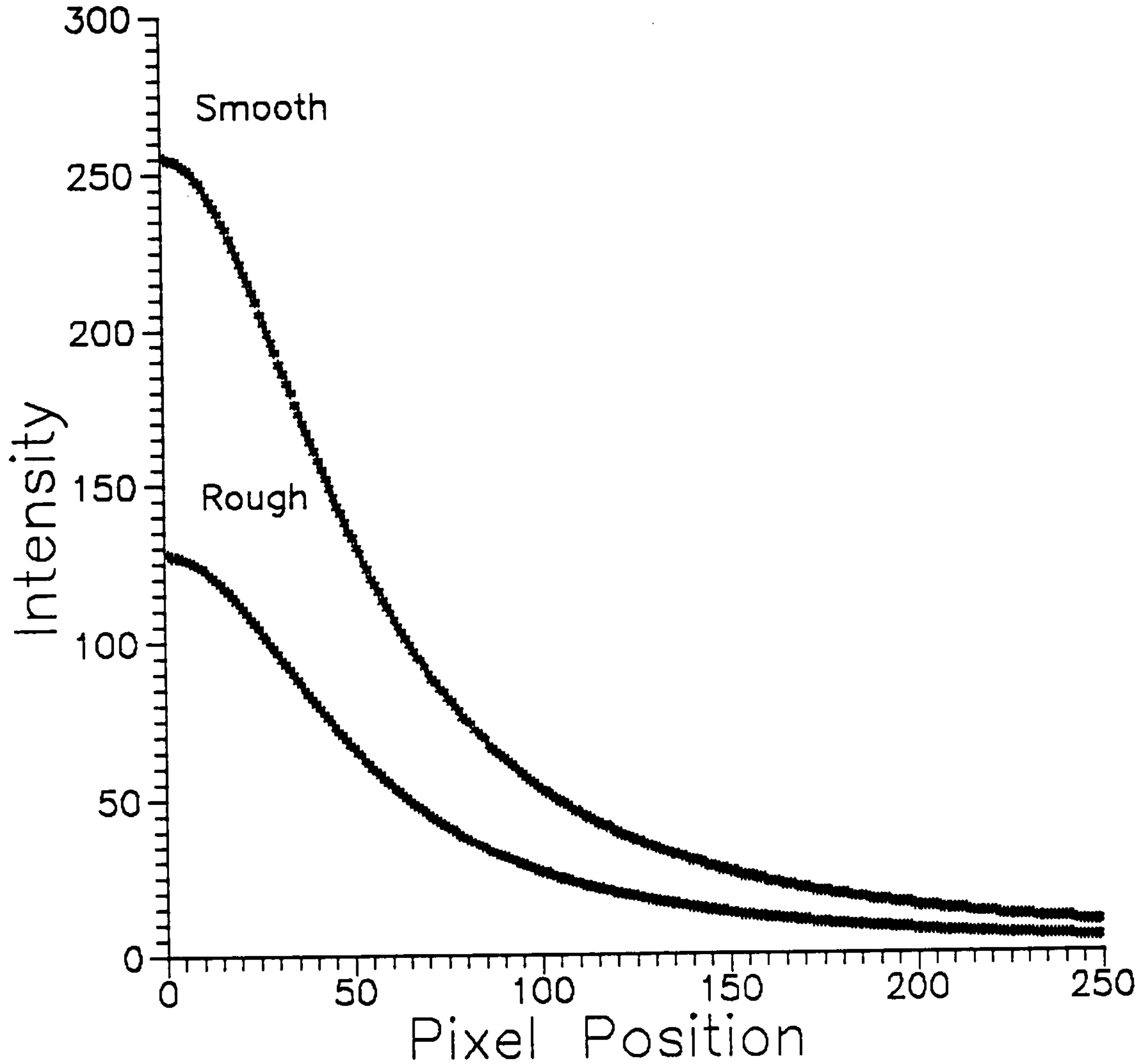

Figure 3.5 Intensity vs Pixel Position for Theoretical Smooth Fiber and Randomly Rough Fiber

as the fiber becomes rough more and more of the light is scattered by the scattering centers, out of the specular beam. The scattering out of the specular beam causes the intensity of the specular streak to decrease. This decrease in intensity is related to the amount of roughness since, as the roughness increases, the number of scattering centers increases thus scattering more and more light out of the specular region. In calculating the roughness coefficient an effort is made to remove areas within the scattering pattern that may contain bad data. These areas are the beam stop, on the far right of the pattern, and the far left edge of the pattern, where edge effects from the screen are present (Figure 3.6). This is accomplished in the program by removing the right most 50 data columns and the left most 25.

The program that calculates the roughness coefficient is the FORTRAN program RC.FOR. The program prompts the user for the name of the actual data file, the summation of the intensity values for the theoretical data, and the starting and ending X,Y coordinates. In addition the program prompts the user for the approximate y-coordinates of the specular region of the actual file. The specular region is equal in height to the diameter of the incident light, i.e. the length of the sample fiber illuminated. The program then sums the intensity values in the specular region of the actual fiber and the intensities for the theoretical smooth fiber. The number of rows summed is controlled by the camera-to-screen distance and is obtained by equation 3-5. The roughness coefficient (RC) is defined by

$$RC=\frac{\sum\sum I_{ij}}{\sum\sum I^{0}_{ij}} \tag{3-9}$$

Where RC is the roughness coefficient, I_{ij} is the summation of the intensity values in the specular region for the actual fiber, and I^{o}_{ij} is the summation of the intensity values for the specular reflection of a theoretically perfect smooth fiber.

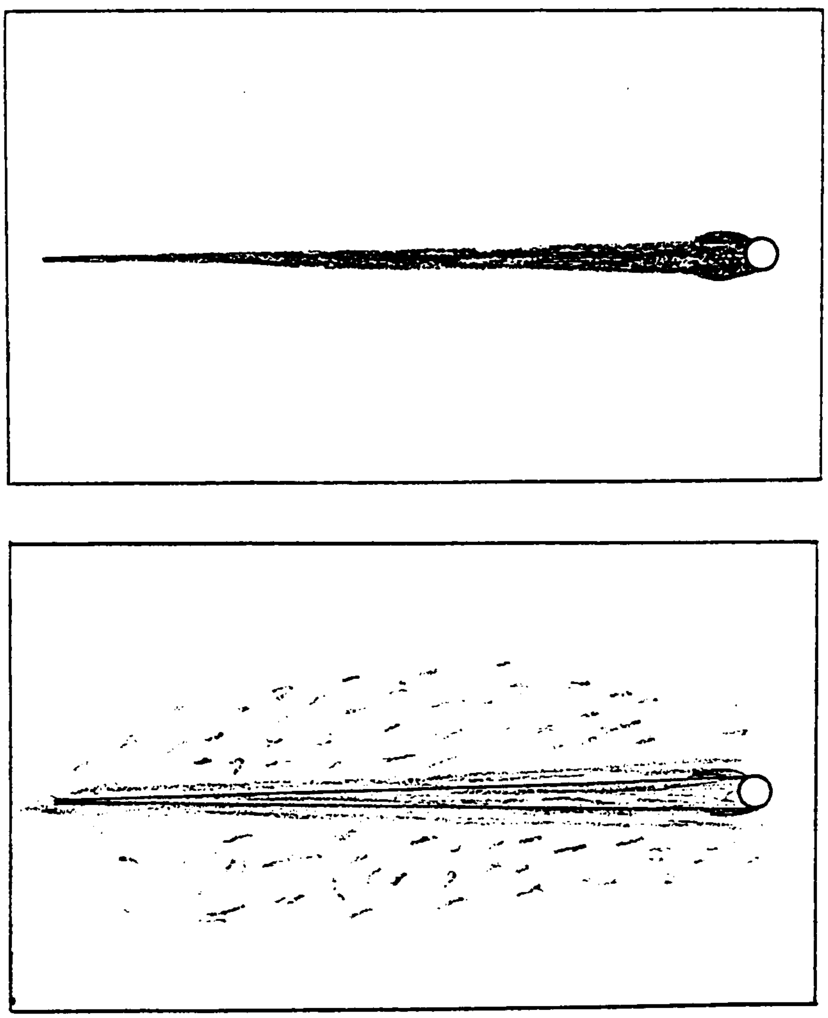

Figure 3.6 Scattering Pattern for Smooth and Rough Fiber

IV. EXPERIMENTAL FIBER SURFACE SCATTERING

4.1 INTRODUCTION

To accomplish the goals set forth for this work, it was necessary to take data of three major types. These data types were necessary to provide information on (i) the effects of equipment parameters on the scattering pattern, (ii) the effects of fiber diameter on the scattering pattern, and (iii) to determine if the surface roughness of a fiber could easily and accurately be obtained from its small-angle back scattering pattern.

4.2 EXPERIMENTAL METHODS

For the purpose of investigating these areas the equipment illustrated in Figure 4.1 was used. The only variables involved were the samples used and equipment parameters. The samples included a surface roughness comparator, stainless steel wires, and various polymer fiber samples. The equipment parameters varied were Camera f-stop, Laser to Sample (LTS) distance, Sample to Imaging Screen (STS) distance, and Imaging Screen to Camera (STC) distance. The small-angle light back scattering system was composed of a 2 mW He-Ne laser serving as a light source. There is a sample holder that allows for 360° rotation about the beam direction. An imaging screen that is composed of Mylar. A vidicon

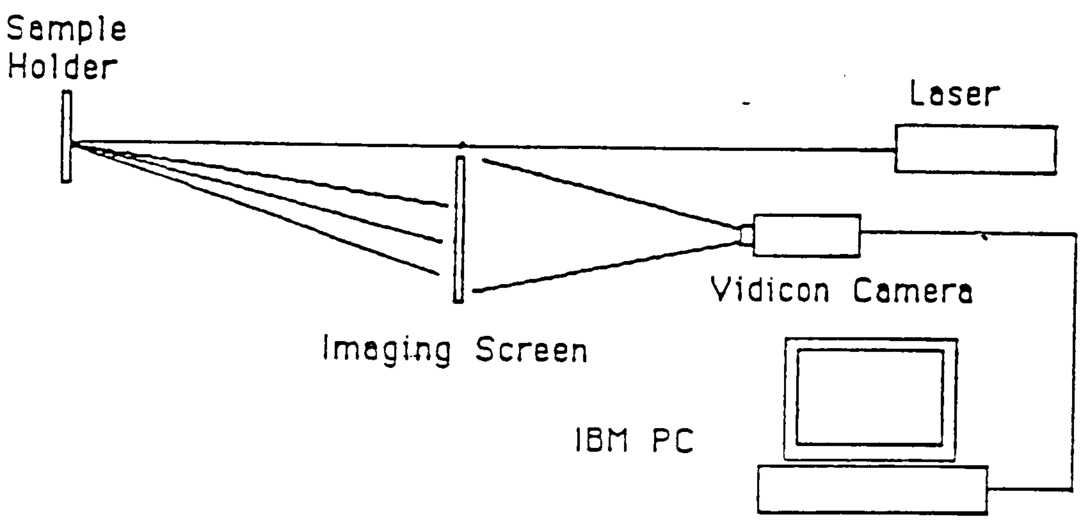

Figure 4.1 SALBS Equipment (Cheng)

camera, to receive the image, connected to an IBM PC equipped with a video digitizer card. It should be noted that with each set of samples the contrast control, on the camera, was adjusted to minimize the number of maximum intensity values recorded.

The data was taken using a wide variety of samples. The samples included a surface roughness comparator, stainless steel wires, polyethylene (PE) fibers, Kevlar fibers, and a variety of Carbon fibers. The comparator was the Surface Roughness Scale - Catalog Number 342X60 made by General Electric. The stainless steel wire samples were manufactured by the Prindle-Fabbri Corporation and consisted of the following diameters 0.012, 0.014, 0.016, 0.018, and 0.022 inches. The Kevlar fibers were DuPont 1140 denier KEVLAR 49 yarn. The Carbon fibers used were provided by DuPont and consisted of P10281-115B 30 MPSI pitch carbon fiber with finish, P10281-115D 130 MPSI pitch carbon fiber, and P10281-115E 60 MPSI pitch carbon fiber samples.

4.2.1 EQUIPMENT PARAMETER EFFECTS

In configuring a small-angle light back scattering system to record data, it is desirable to obtain the highest quality image possible. To this extent it is necessary to determine the optimum equipment configuration or configurations. This configuration determination should not be thought of as a method of fine tuning the image quality from sample to sample but rather a means of optimizing all sample images recorded.

Adjustments from sample to sample should be made using the camera's focus, black, and contrast tuning abilities. In an attempt to determine this optimum configuration samples were recorded varying the different equipment geometry parameters.

To study the effects of camera f-stop a surface roughness comparator was used. Samples were recorded at f-stops of 2, 4, and 8 using root-mean-square roughnesses of 8, 32, and 63 microinches. To study the effects of LTS, STS, STC distances samples from the 60 μm polyethylene (PE) fiber and the 0.012 inch diameter stainless steel wire were used. Samples using the PE were recorded for the LTS study with laser to sample distances varied between 91 and 111 cm in 5 cm increments, with a STS of 10 cm and a STC distance of 70 cm. The sample to imaging screen distances were varied between 10 and 30 cm in 5 cm increments for the STS set with a LTS of 111 cm and a STC of 70 cm. The final set of equipment parameter data taken, using the PE samples, were for the STC study. The imaging screen to camera distances were varied between 70 and 90 cm, again, in 5 cm increments with a LTS distance of 111 cm and a STS of 10 cm. For all PE samples used in studying the LTS, STS, and STC distance effects the f-stop of the camera was set at a setting of 2. For the stainless steel wire samples the LTS study used laser to samples distances of 91 to 111 cm varied in 5 cm increments, a STS distance of 10 cm and a STC distance of 60 cm. The distances in the STS study were varied in 5 cm increments between 10 and 30 cm with a LTS of 111 cm and a STC of 60 cm. The final set recorded using the stainless steel wire was for the sample to screen distance study with STC distances ranging from 65 to 85 cm varied in 5 cm increments, with a LTS of 111 cm and a STS of 10 cm. For all geometry parameter samples the camera f-stop was set at a setting of 2.

4.2.2 FIBER DIAMETER EFFECTS

Also of interest was the effect that varying the fiber diameter has on the scattering pattern. If identical materials, having the same surface roughness, but of different diameters are studied the resultant calculated roughness should be the same. It is known that as the fiber diameter increases the scattering pattern should go from a streak, the fiber scattering pattern (Figure 4.2), to a dot, at an infinite diameter or perfectly flat sample (Figure 4.3). Stainless steel was chosen due to the 100 atom thick oxide coating it possesses giving it the appearance of being smooth.

In an effort to examine how the fiber diameter effects the scattering pattern. Back scattering patterns were recorded using the stainless steel wire samples. The diameter of the steel fibers ranged from 0.012 to 0.022 inches. The scattering equipment components were located at the following locations; camera 20 cm, screen 90 cm, laser 9 cm, sample 101 cm, with a camera f-stop setting of 4. The settings give a LTS distance of 92 cm, a STS distance of 11 cm, and a STC distance of 70 cm.

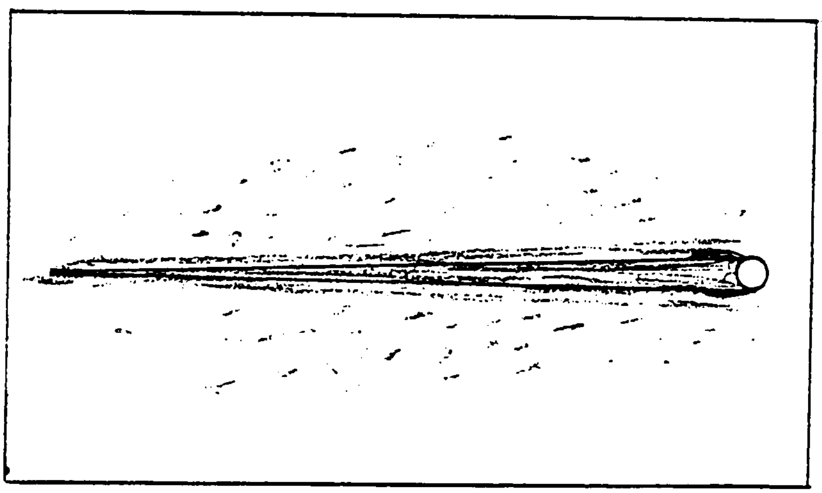

Figure 4.2 General Scattering Pattern from a Fiber

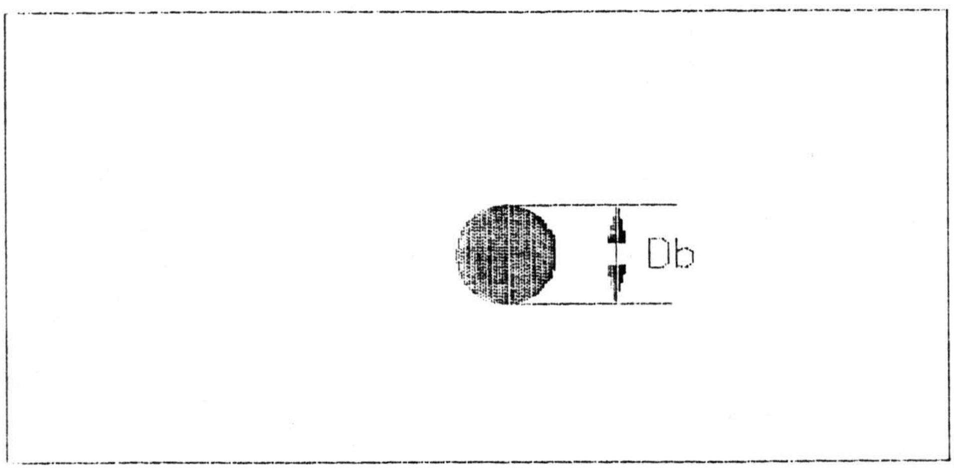

Figure 4.3 General Scattering Pattern from a Perfectly Flat Surface

4.2.3 SURFACE ROUGHNESS DETERMINATION

In order to determine the surface roughness of a sample the specular reflection region and the non-specular scattering region must be determined from the total integrated small-angle back scattering pattern. As previously stated, an infinitely smooth material will produce only specular reflection, as the material surface becomes rough, non-specular scattering will appear and the pattern will become more diffuse. Since the amount of light must be conserved as the non-specular scattering appears, the amount of light within the specular region must decrease. It is this decrease in the specular region from a perfectly smooth sample to a rough sample that is the basis for the surface roughness coefficient.

4.2.3.1 Specular Scattering Determination

In the past, one of the most common methods of determining the specular region of a integrated scattering pattern was to 'eye' the pattern and 'best guess' the specular region. However, this method is prone to considerable human error, especially from one person to another. It was, therefore, desirable to develop a reproducible method to experimentally determine specular scattering. The experimental method used was to take the same fiber used for the integrated scattering pattern and "wet" the surface with a liquid of the same refractive index. In theory this process should have made the fiber appear smooth to the incident beam. Using this method, data was taken using the PE fibers, PP fibers, Kevlar fibers, and carbon fiber samples. The wetting agent used was Corgille Non-drying Immersion Oil.

4.2.3.2 Integrated Scattering Patterns

It was desirable to obtain a wide variety of data sets to test the reliability and accuracy of the surface roughness coefficient. Data was taken using PE, Kevlar, and two carbon fiber samples. The equipment component positions were as follows; camera 20 cm, sample 110 cm, screen 90 cm, and laser 20 cm. These component positions gave parameter distances of 90 cm for the LTS, 20 cm for the STS, and 70 cm for the STC. An f-stop setting of 2.8 was used for the PP, an f-stop setting of 1.4 for carbon fiber 115B, and an f-stop setting of 2 was used for the Kevlar, PE, carbon 115D, and carbon 115E samples. In addition to these patterns, samples were recorded using the surface roughness scale, produced by General Electric, at an incident angle of 45°. Patterns were recorded for roughness values of 4, 8, 16, 32, and 63 micro inches root-mean-square average roughness. The equipment components were positioned as follows the camera at 50 cm with an f-stop of 2, the screen at 90 cm, the laser at 9 cm, and the sample at 100 cm. This gave an LTS of 91 cm, an STS of 10 cm, and an STC of 40 cm. The STC distance was decreased in an effort to maximize the number of pixels within the specular region. In addition to the components illustrated in Figure 4.1 a polarizer was placed in front of the laser. This was necessary due to the fact that the surface roughness scale was metallic and all the recorded intensities were maximum values. The polarizer was then adjusted until the smoothest sample produced an image where the majority of the pixels, within the specular region, were near the maximum intensity value of 255. These patterns were then used to determine the applicability of the roughness coefficient measurement.

In addition, a series of experiments were performed to determine to reliability and reproducability of the small-angle light back scattering patterns and the calculated roughness coefficient. Patterns were recorded using the roughness comparator with the following three equipment configurations: (1) camera 20 cm, sample 120 cm, laser 20 cm, and screen 100 cm (2) camera 30, sample 120 cm, laser 20 cm, screen 100 cm (3) camera 20 cm, sample 120 cm, laser 20 cm, and screen 90 cm. The first configuration was used on one day and the other two were used the next day. For each set of measurements the camera's contrast and gain setting were used to calibrate the readings, ten images were recorded at each position.

V. RESULTS AND DISCUSSION

5.1 INTRODUCTION

The discussion of the results obtained in this work is divided into two major sections. Those sections being equipment and sample parameters and surface roughness determination. The equipment parameters sections deals with various equipment setups and parameters and how they affect the recorded integrated scattering pattern. The roughness determination section reviews the data collected in an attempt to study the reliability of the proposed roughness coefficient and the method of graphical representation of the sample surface.

5.2 EQUIPMENT PARAMETERS

The purpose of this section is to evaluate the data recorded for the various geometry configurations studied. It is hoped that this data will lead to the determination of an optimum equipment configuration or configurations. The parameters of interest are Laser-to-sample distance, Sample-to-screen distance, Screen-to-camera distance, Camera f-stop, and fiber diameter. As stated before the geometry parameters are not meant to be a method of fine tuning an individual sample pattern, but rather a means of obtaining a digitized pattern of optimal picture quality and usefulness for all samples.

The data obtained by varying the Laser-to-sample distance is presented in Table 5.1 and is illustrated in Figure 5.1. Figure 5.1 shows a parabolic type variation in the summed total integrated scattering patterns for the various Laser-to-sample distances examined. This type of dependency is not expected, however it is believed that this variation is due to the cross-sectional characteristics of the beam and not the Laser-to-sample distance. If the beam is viewed as in Figure 5.2, it can be seen that the intensity distribution of the beam is Gaussian, with the beam's center having the greatest intensity. This is not important if the samples studied are wider or have a greater diameter than the incident beam, since all samples would 'see' the same distribution. However, if the sample's diameter, or width, is smaller than the incident beam the placement of the sample within the beam alters the intensity that strikes the sample and thus alters the intensity of the scattered or reflected light.

The total summed scattering patterns obtained from the various Sample-to-screen distances examined, also show intensity variations. This data is presented in Table 5.2 and represented in Figure 5.3. The data reveals that at the smaller Sample-to-screen distances the summed intensities are smaller and increase with increasing STS distances until they maximize and then decrease with further increases in distance. This behavior can be explained by examining how a pattern forms with respect to the imaging screen. When the sample is placed close to the screen the pattern is more compact and the pattern density is greater than the pixel of the camera, therefore fewer high intensity points are recorded. When

Table 5.1: Summed Total Integrated Scattering Patterns as a Function of Laser-to-Sample Distance

Laser-to-Sample (cm)	PE	Stainless Steel
90	95085	132534
95	68807	116295
100	68807	107529
105	107323	106532
110		116185

Table 5.2: Summed Total Integrated Scattering Patterns as a Function of Sample-to-Screen Distance

Sample-to-Screen (cm)	PE	Stainless Steel
10	65710	113755
15	92564	121548
20	99936	121548
25	68461	101831
30		86471

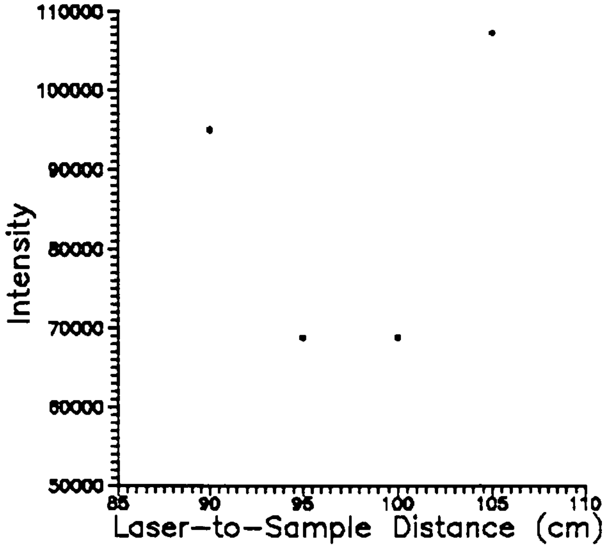

(a)

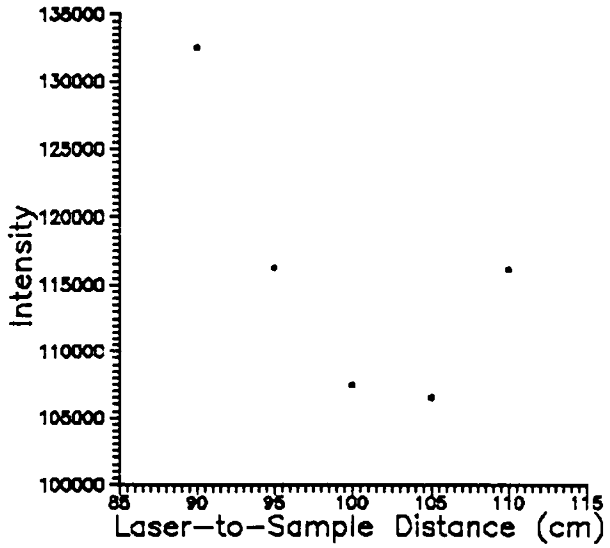

(b)

Figure 5.1 Summed Total Integrated Scattering Patterns as a Function of Laser-to-Sample Distance
(a) PE
(b) Stainless Steel

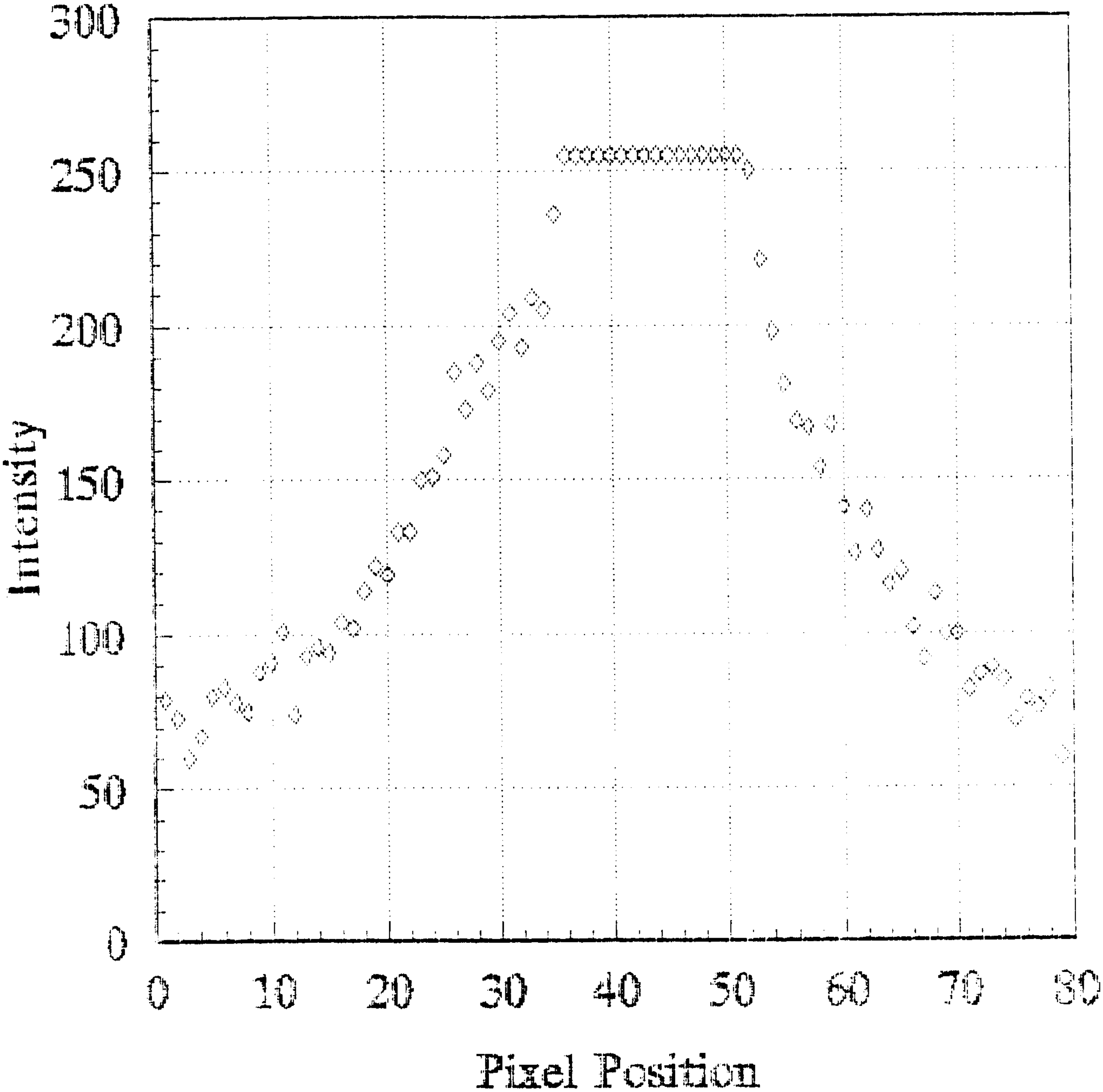

Figure 5.2 Cross Section of Incident Beam

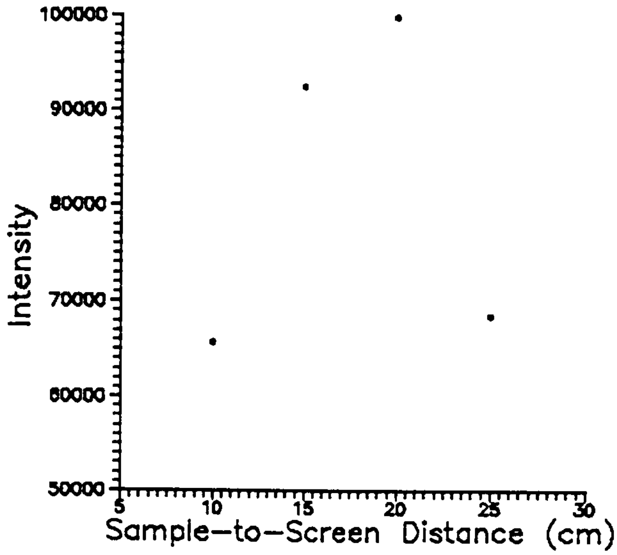

(a)

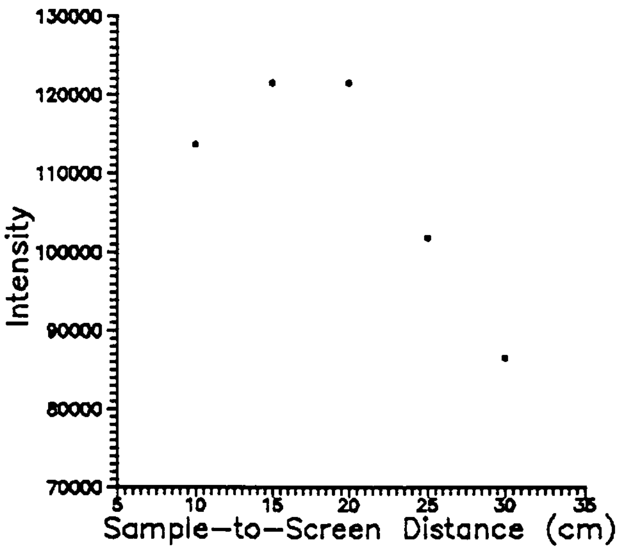

(b)

Figure 5.3 Summed Total Integrated Scattering Patterns as a Function of Sample-to-Screen Distance
(a) PE
(b) Stainless Steel

the sample-to-screen distance is increased the scattered pattern becomes less compact and high intensity values are encountered farther away from the beam stop. This behavior continues until the pattern density is optimized with the camera's pixel density. After this point is exceeded the scattered pattern's density becomes less than the camera's pixel density and lower intensity voids begin to appear in the pattern. Also the reflected and scattered intensities start to decrease as a function of the STS distance squared and the camera records fewer high intensity values.

The behavior of the scattered patterns as a function of the Screen-to-camera is similar to that seen for the Sample-to-screen patterns. That is to say that the patterns recorded at the smaller STC distances show smaller summed total intensities, increasing as the distance increases up to a maximum and then decreasing with continued increases in the STC distance. This data is presented in Table 5.3 and illustrated in Figure 5.4. The reasoning behind the behavior of the patterns as a function of the Screen-to-camera distance is analogous to that of the Sample-to-screen behavior. That is primarily the relationship between the camera's pixel density and the pattern's intensity density with the distance squared effect becoming important as the distance increase beyond the optimum STC distance.

The data taken to determine the effect of the camera's f-stop on the scattering image is represented in Figure 5.5 and listed in Table 5.4. The data of the summed total integrated scattering pattern shows that as

Table 5.3: Summed Total Integrated Scattering Patterns as a Function of Screen-to-Camera Distance

Screen-to-Camera (cm)	PE	Stainless Steel
65		106653
70	65710	106045
75	79919	105692
80	96651	109358
85	102676	106637
90	98999	

Table 5.4: Summed Total Integrated Scattering Patterns as a Function of Camera f-stop

Surface Comparator (rms / micro inches)	f - stop		
	2	4	8
32	1,267,615	299,729	54,779
63	1,752,744	499,572	98,285
125	1,240,338	376,400	80,089

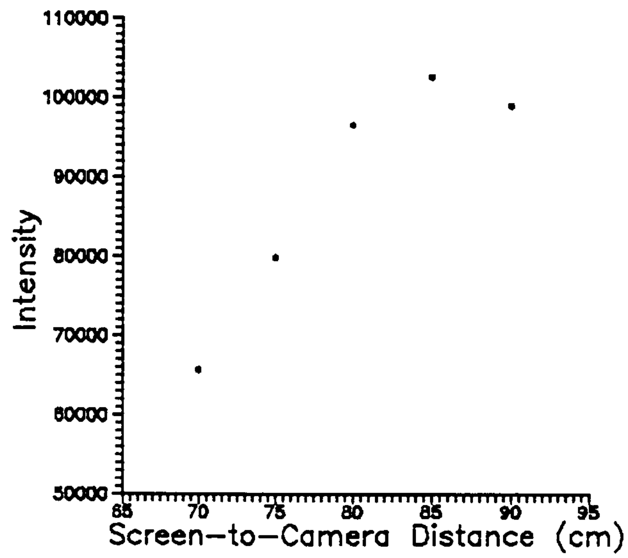

(a)

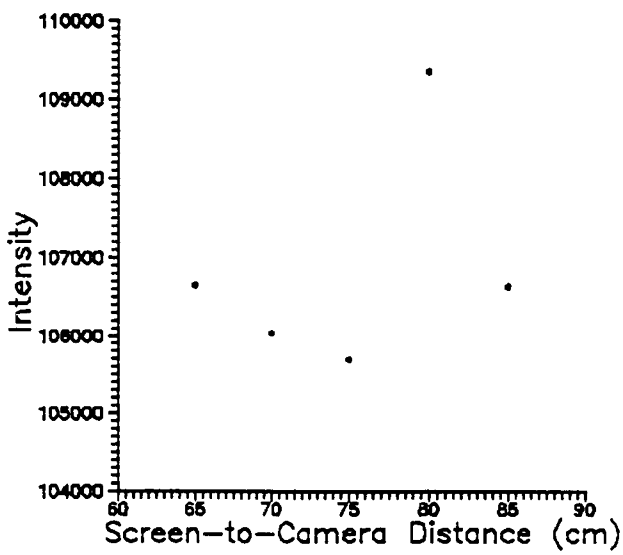

(b)

Figure 5.4 Summed Total Integrated Scattering Patterns as a Function of Screen-to-Camera Distance
(a) PE
(b) Stainless Steel

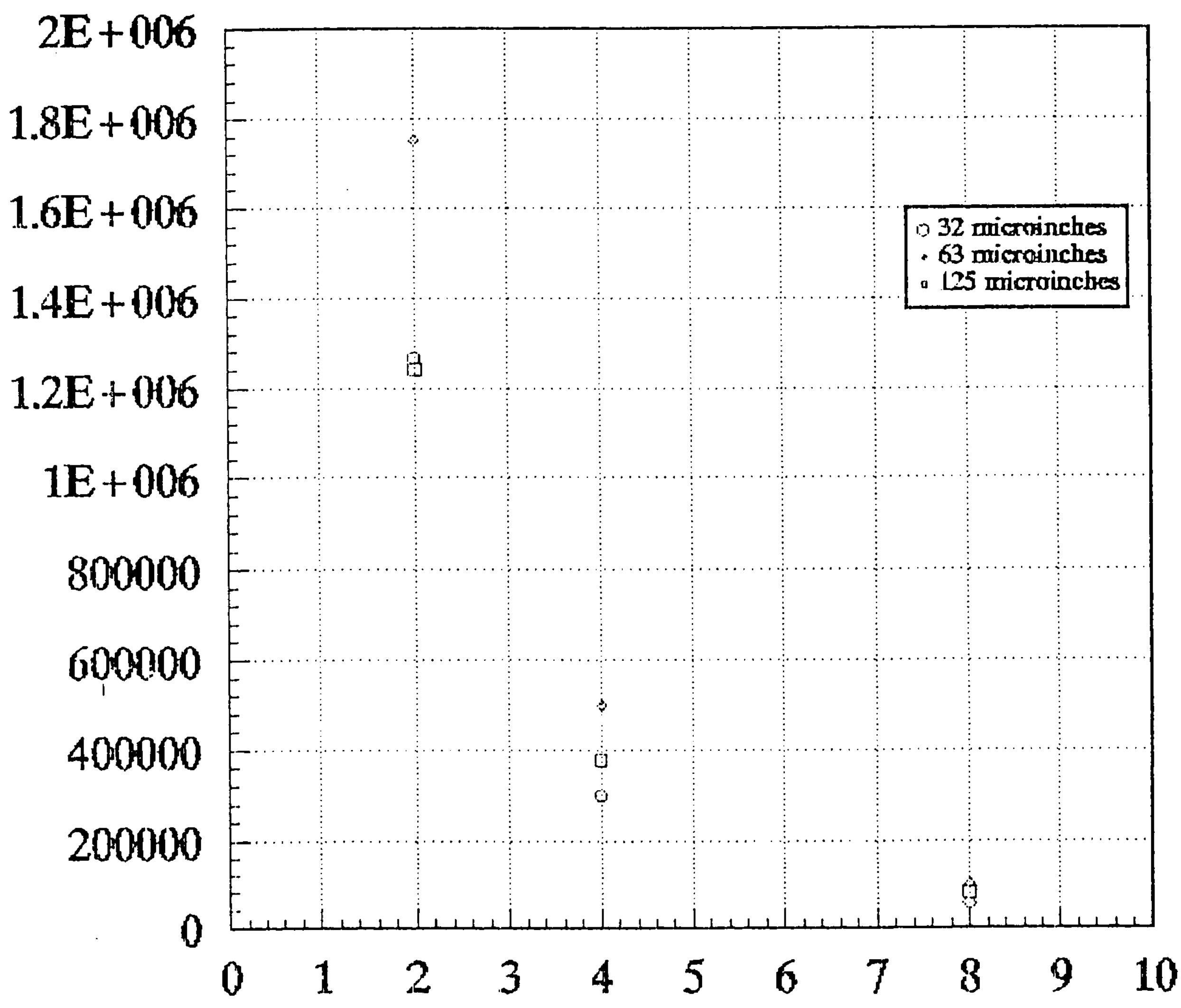

Figure 5.5 Summed Total Integrated Scattering Patterns as a Function of Camera f-stop

the f-stop is increased the summed intensities decrease. The behavior experienced is the type expected, since as the f-stop is increased the amount of the pattern seen by the camera decreases.

The last area investigated was the effect of fiber diameter on the scattering pattern. The data obtained shows variation of the summed intensities with changes in diameter, however this behavior is not expected. The data in Table 5.5 and illustrated in Figure 5.6 does not show a constant pattern, that is to say that an increase in fiber diameter does not show a constant increase or decrease in the summed intensities. It is therefore suggested that the variations are due to the cross-sectional characteristics of the incident beam and not changes in the fiber diameter.

The findings of the equipment geometry and parameters investigation suggest that the arrangement of the equipment are of greater importance than that of the camera f-stop or the fiber diameter. This is especially true for the Sample-to-screen distance, the Screen-to-camera distance, and the position of a fiber sample within the incident beam.

5.3 ROUGHNESS DETERMINATION

In an effort to provide support to the notion that the surface roughness of a sample can be accurately determined by small-angle light back scattering and can be represented graphically using Fourier

Table 5.5: Summed Total Integrated Scattering Patterns as a Function of Fiber Diameter

Fiber Diameter (inches)	Intensity
0.012	211,971
0.014	224,100
0.016	260,694
0.018	137,198

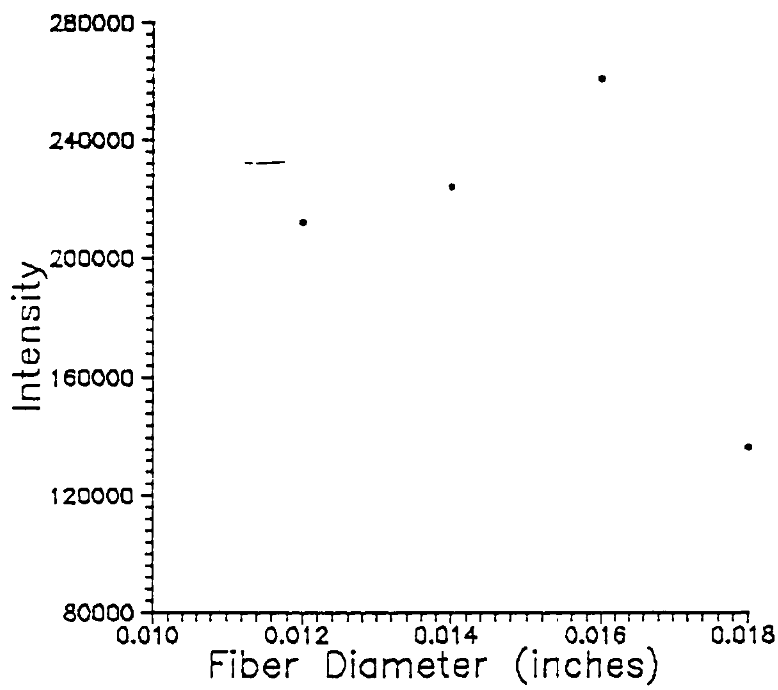

Figure 5.6 Summed Total Integrated Scattering Patterns as a Function of Fiber Diameter

transforms the following analysis is provided. The data taken in an effort to provide information about the reproducability of the roughness coefficient is presented in Table 5.6. The first set of data produced an average roughness coefficient of 0.96 with a standard deviation of 0.01. The second set gave an average roughness coefficient of 0.96 with a standard deviation of 0. The third set of data produced an average roughness coefficient of 0.97 with a standard deviation of 0.1. When the three sets are compared the average roughness coefficient obtained was 0.96 with a standard deviation of 0.01. The data obtained from the surface roughness comparator yielded roughness coefficients ranging from 0.99, for a rms roughness of 4 microinches, to 0.02, for a rms roughness of 63 microinches. The data is presented in Table 5.7 and represented in Figure 5.7. In examining Figure 5.7 it is seen that the data can be described by equation 5.1.

$$RC=1.47\exp(-0.0286rms) \tag{5-1}$$

The analysis of equation 5.1 shows an error sum of squares of 0.025. If however, the data is plotted without the roughness coefficient obtained for the 63 microinches r.m.s. roughness as in Figure 5.8 the data can be described by equation 5.2.

$$RC=1.21\exp(-0.0220rms) \tag{5-2}$$

Table 5.6 Reproducability of the Calculated Roughness Coefficient

Image	Calculated Roughness Coefficient Data Set 1	Data Set 2	Data Set 3
1	0.95	0.96	0.97
2	0.96	0.96	0.96
3	0.96	0.96	0.97
4	0.97	0.96	0.97
5	0.96	0.96	0.96
6	0.96	0.96	0.96
7	0.97	0.96	0.97
8	0.97	0.96	0.97
9	0.96	0.96	0.96
10	0.96	0.96	0.97

Table 5.7: Roughness Coefficients of Standard Roughnesses Represented on a Surface Roughness Comparator

Root-mean-square Roughness	RC
4	0.99
8	0.81
16	0.54
32	0.24
63	0.02

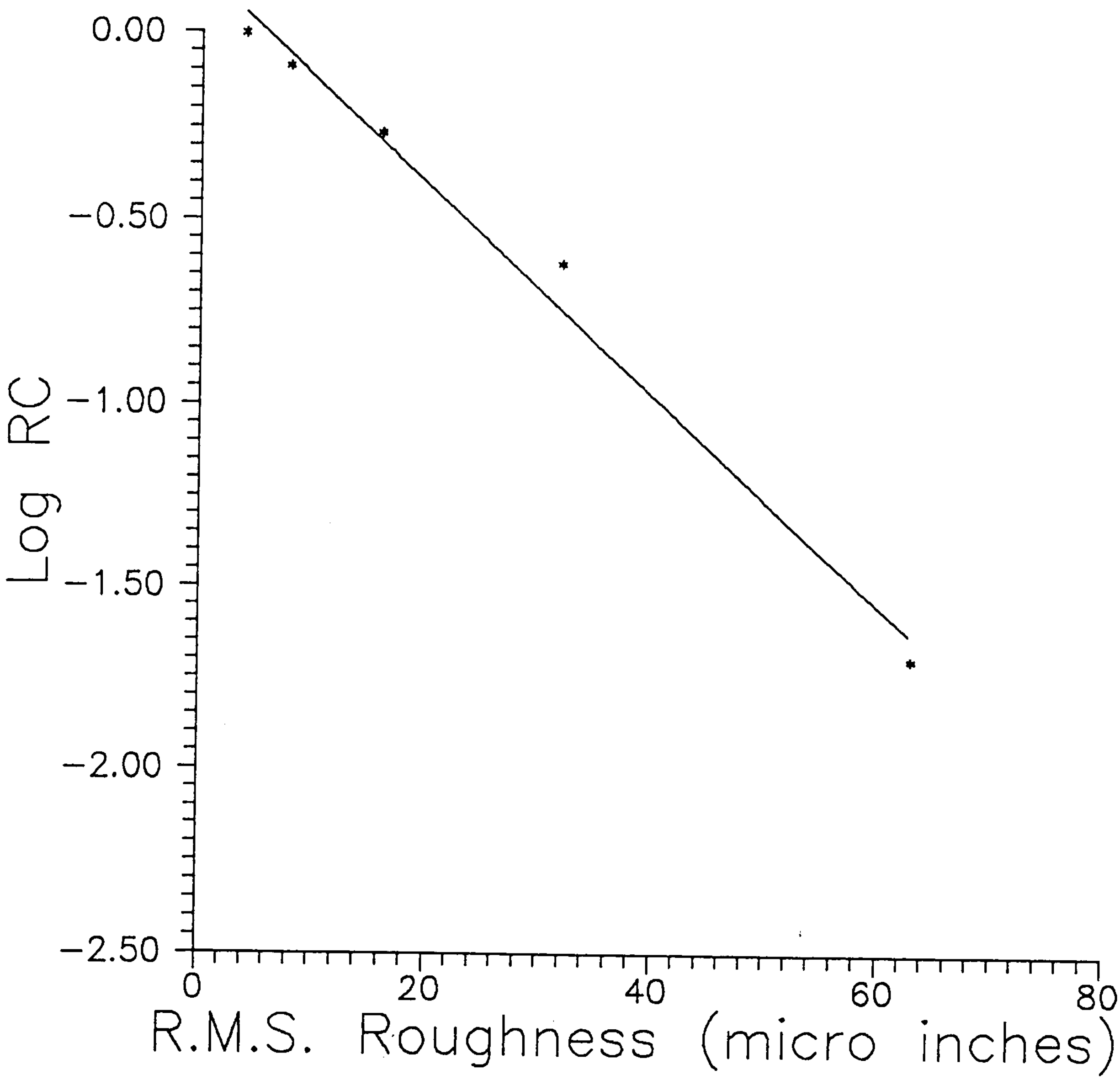

Figure 5.7 Roughness Coefficients of Standard Roughnesses Represented on a Surface Roughness Comparator

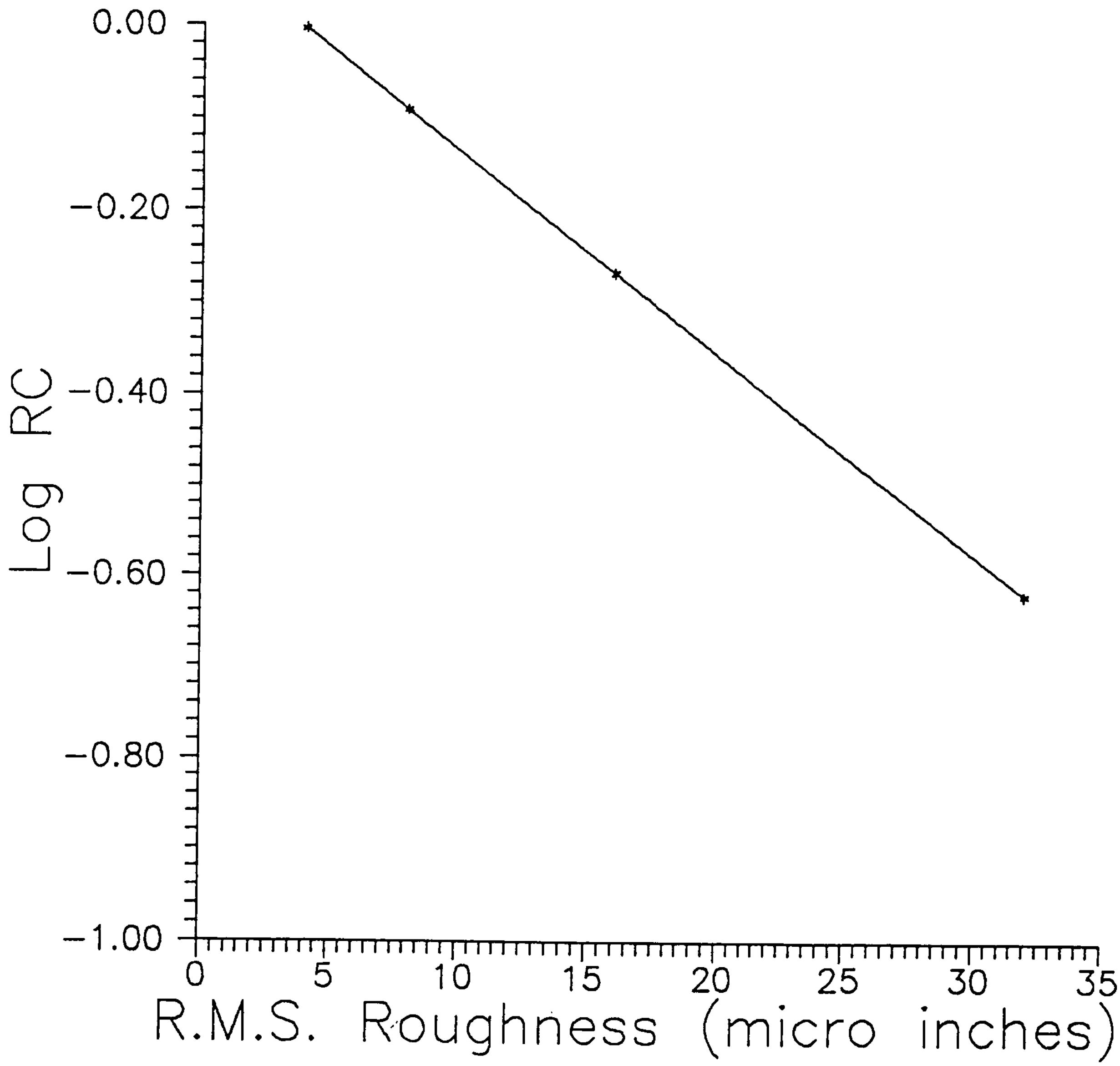

Figure 5.8 Roughness Coefficients of Standard Roughnesses Represented on a Surface Roughness Comparator (Without 63 rms roughness)

The analysis of equation 5.2 shows an error sum of squares of 4.0 E-7. Table 5.8 list RC values for a variety of polymer and carbon fibers. It is important to note that these values are relative to each other and can not be directly related to the values for the surface roughness comparator. This is due to the fact that the equipment was adjusted to give useful patterns for the metal samples. If the equipment had not been adjusted the images produced by the metal samples would have contained primarily maximum intensity values and would have been useless for the calculation of the roughness coefficients.

Fourier transforms were performed on the patterns recorded from the surface roughness comparator and the patterns obtained from the carbon and polymer fibers. The Fourier transformed patterns were then plotted and are presented in Figures 5.9a - 5.9h. The plots show a strong correlation with the known surface roughness values for the roughness comparator. Notice how the peak heights and base widths change with an increase in known surface roughness. The Fourier transformed fiber images show agreement with the magnitude of the calculated surface roughness coefficient.

Table 5.8: Roughness Coefficients of Various Fibers

Fiber	RC
Polyethylene	0.79
Kevlar	0.14
Carbon (115-D)	0.27
Carbon (115-E)	0.14

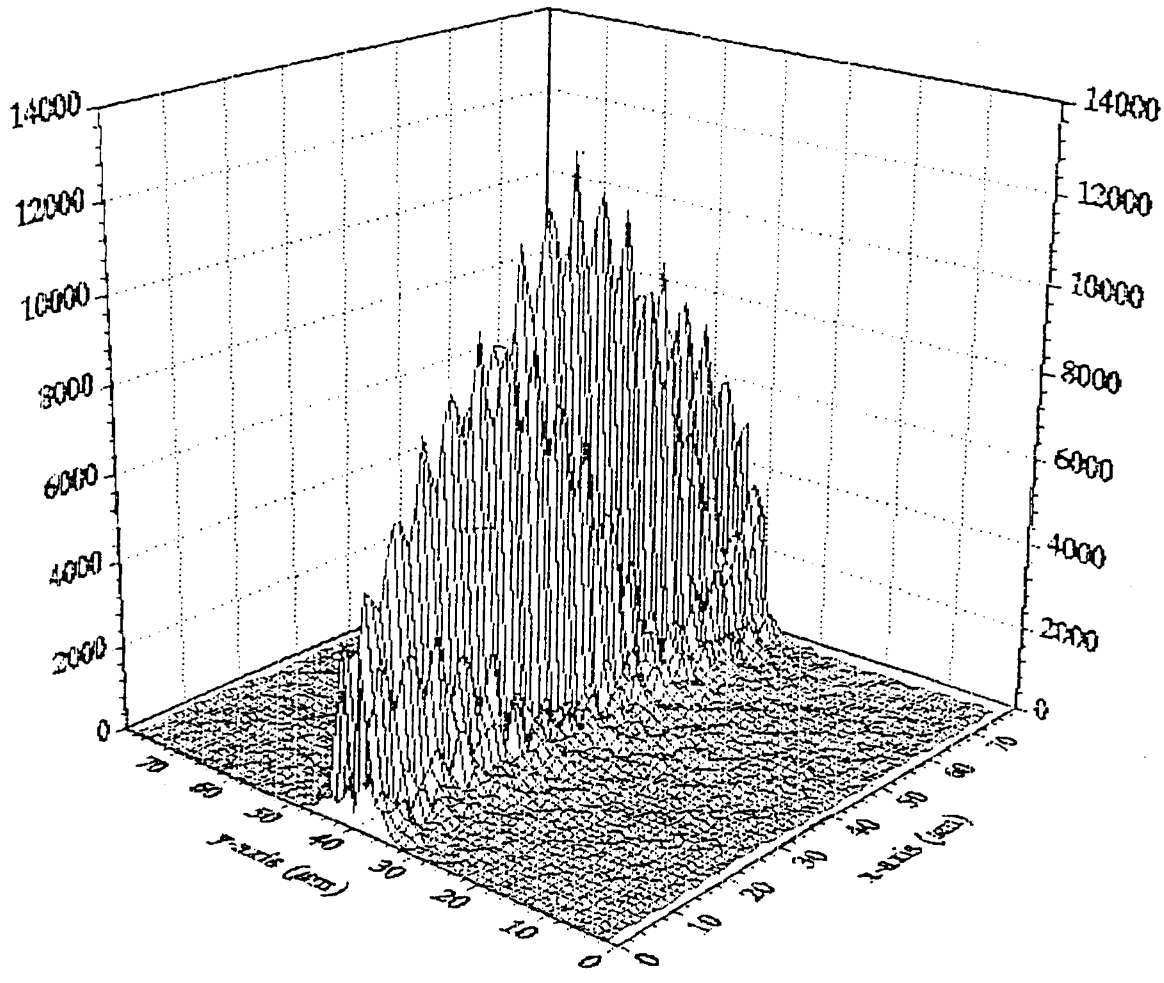

a. 8 micro inches rms roughness

Figure 5.9 Fourier Transformed Surface Roughness Pattern

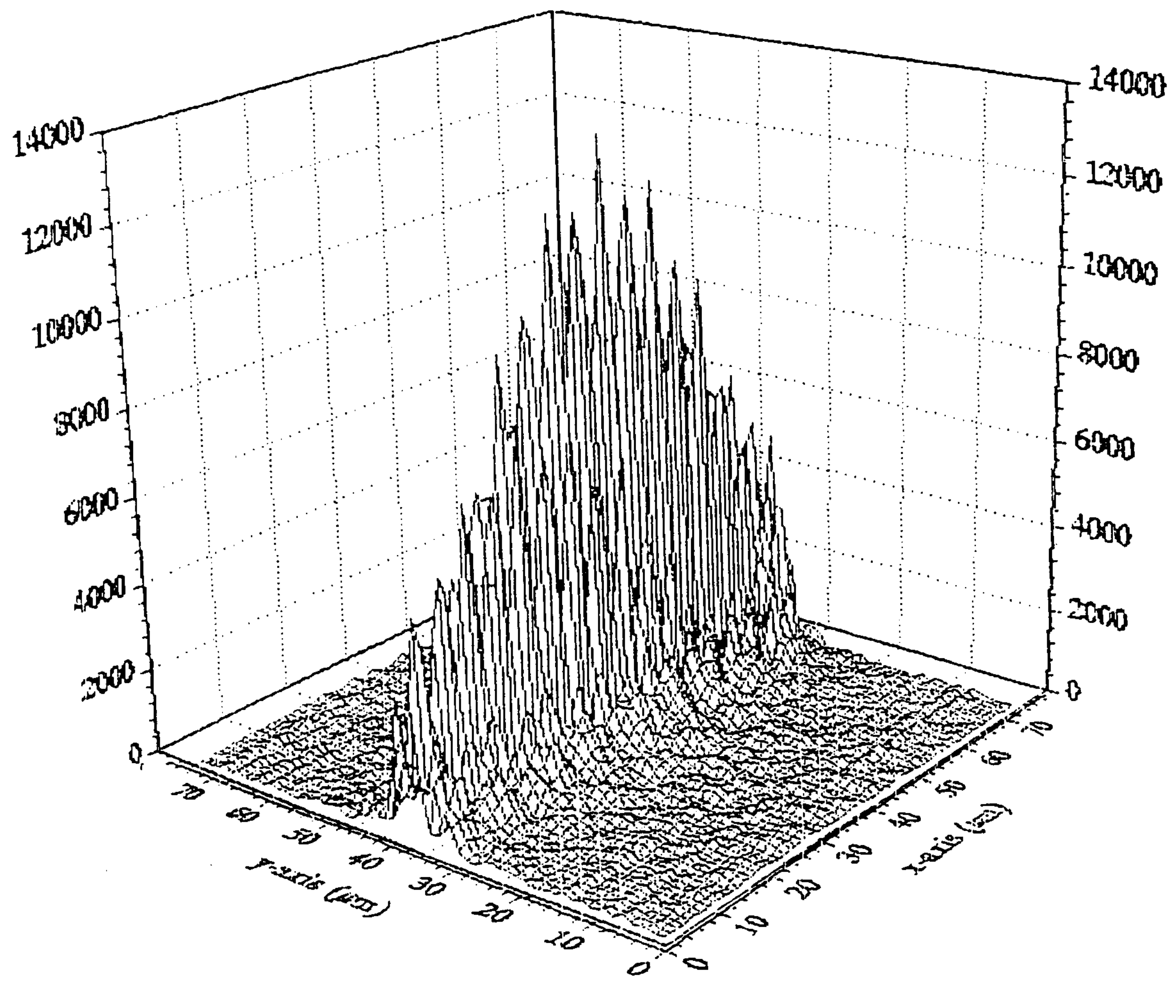

b. 16 micro inches rms roughness

Figure 5.9 (continued)

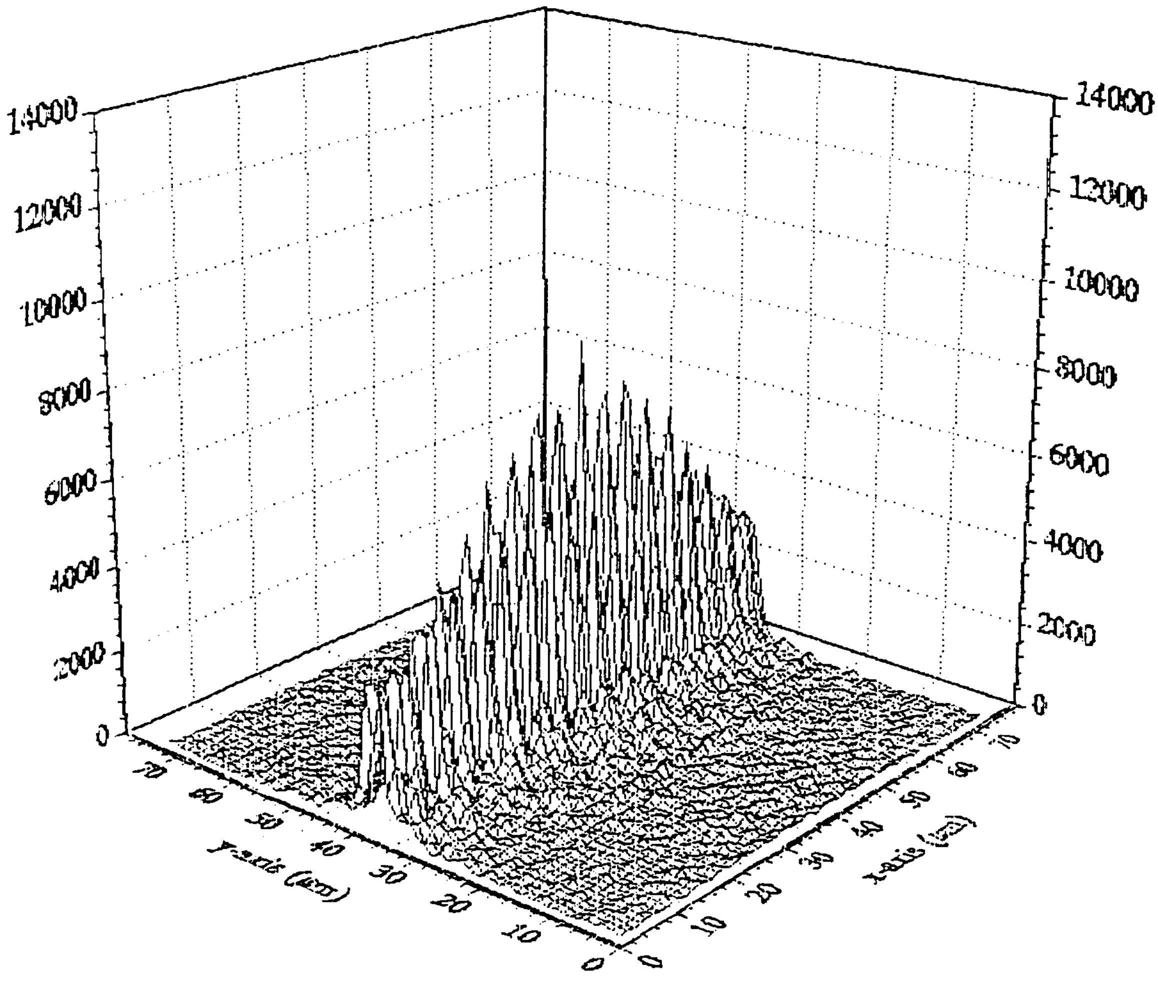

c. 32 micro inches rms roughness

Figure 5.9 (continued)

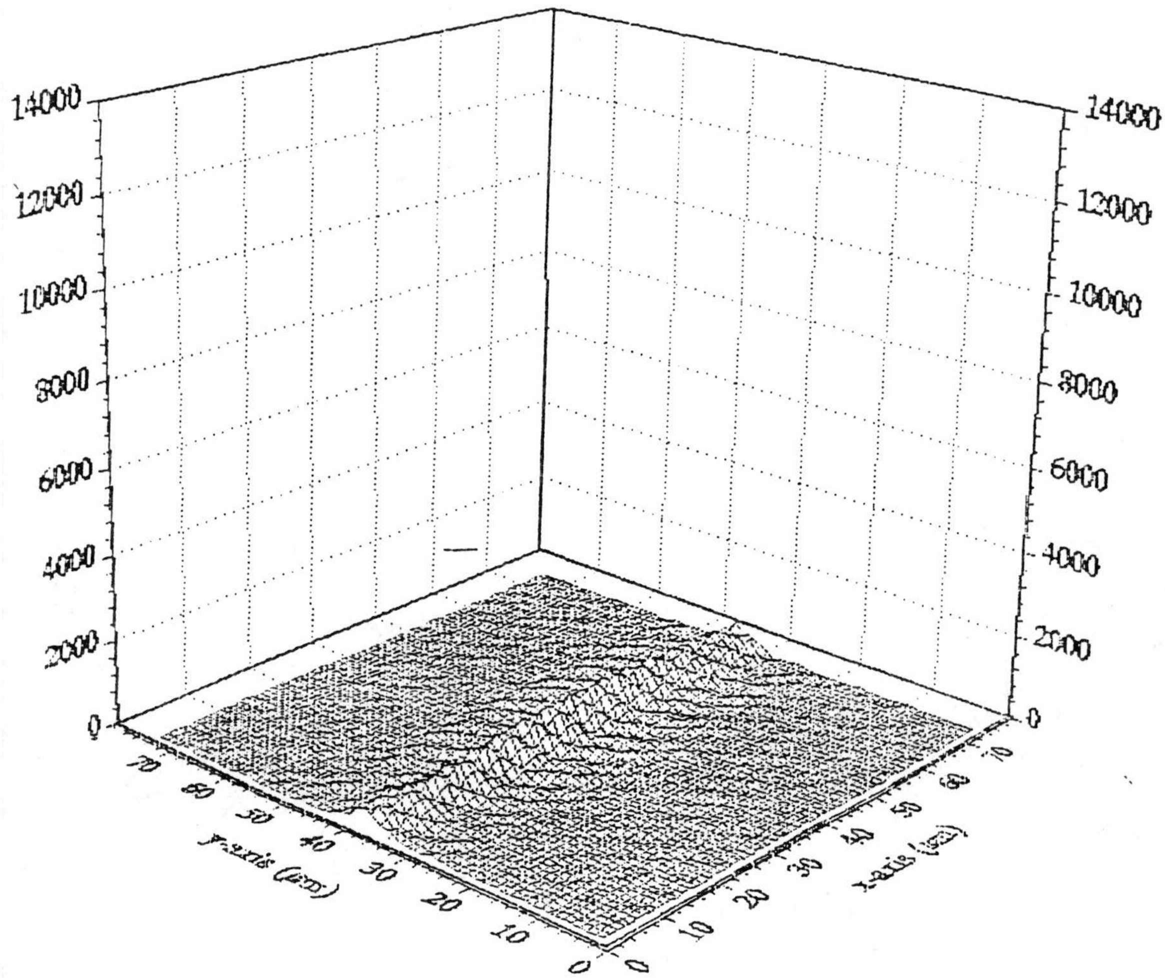

d. 63 micro inches rms roughness

Figure 5.9 (continued)

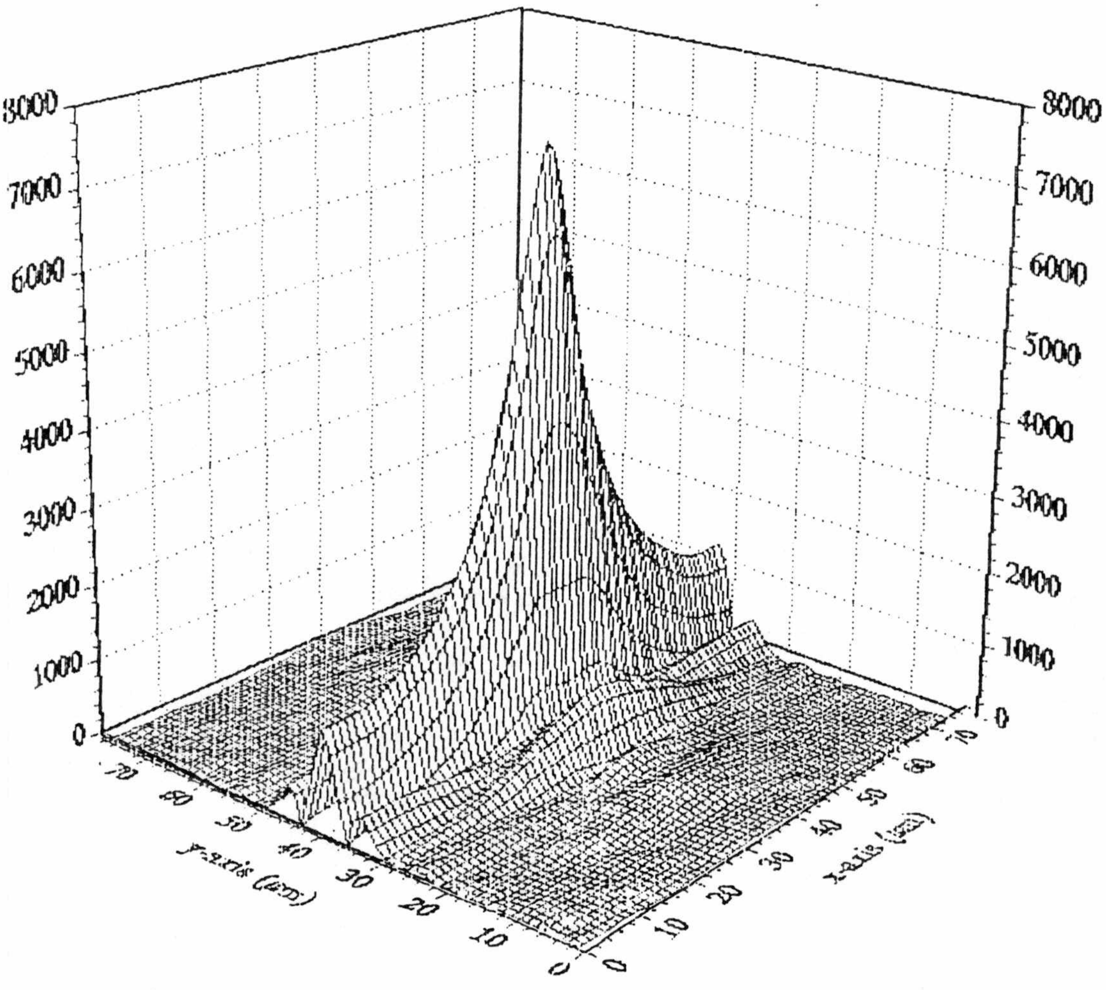

e. PE

Figure 5.9 (continued)

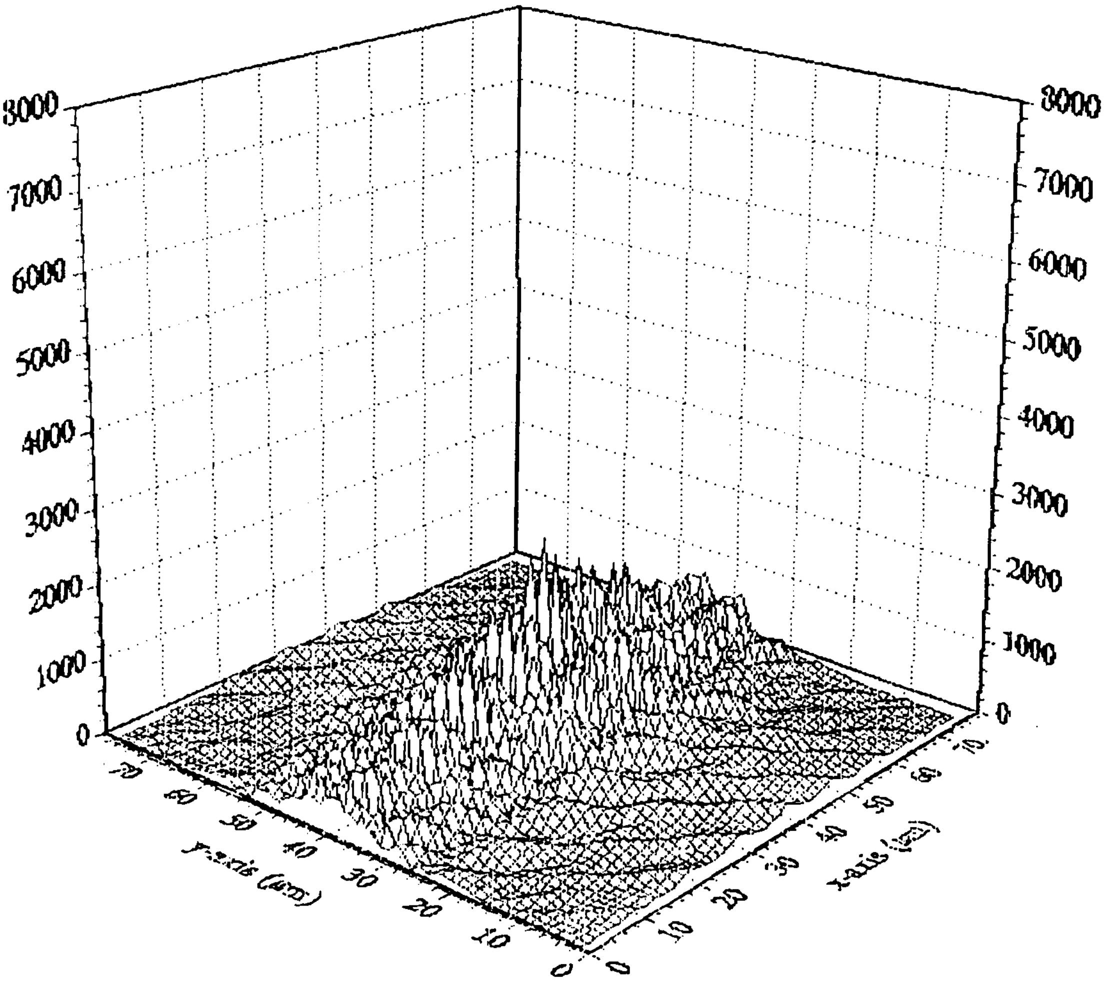

f. Kevlar

Figure 5.9 (continued)

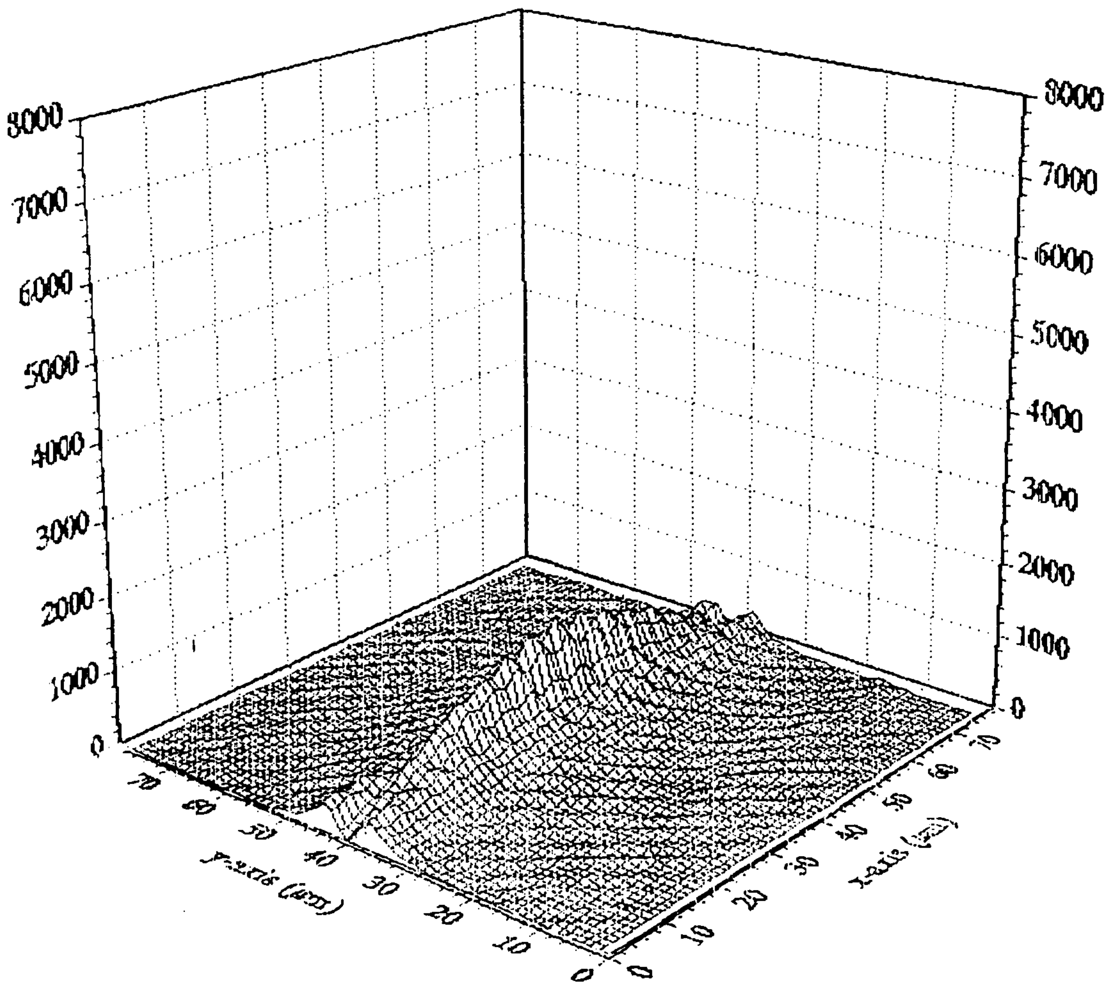

g. Carbon Fiber 115-D

Figure 5.9 (continued)

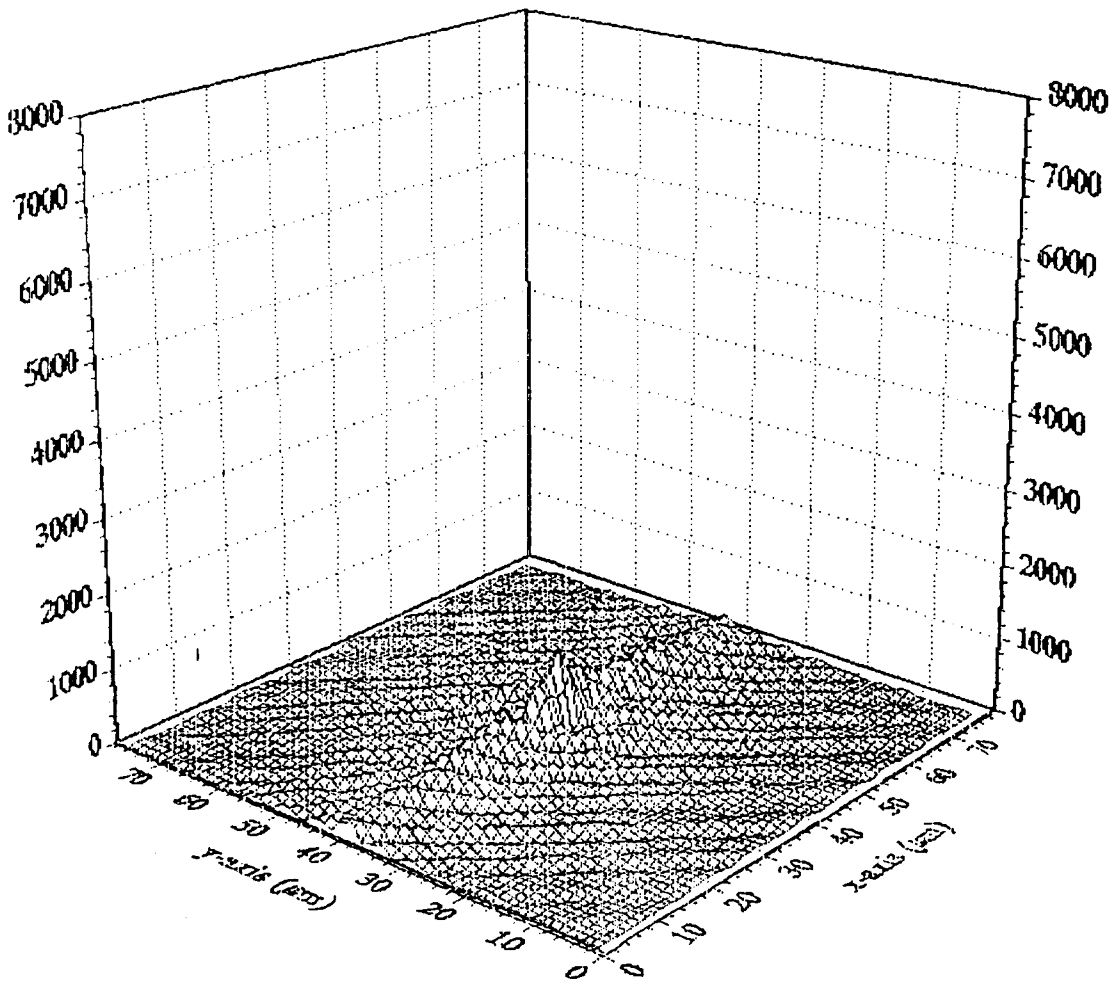

h. Carbon Fiber 115-E

Figure 5.9 (continued)

VI. CONCLUSIONS

Three conclusions can be drawn from the data gathered in this work. It is evident from the data that there exists a range of optimal equipment configurations. In addition, it is apparent that the small-angle light back scattering pattern is strongly related to the surface roughness of the sample. Finally the surface character of a sample can be represented by the Fourier transformed small-angle light back scattering pattern.

From the data gathered, for the purpose of determining the optimum equipment arrangement, the following equipment separation distances are recommended. The laser-to-sample distance should be less than 90 cm. The sample-to-screen distance should not be less than 15 cm nor greater than 25 cm, with an optimum distance of around 20 cm. The screen-to-camera distance should be located between 80 and 90 cm. However, the STC should be decreased if more detailed information about the specular region is desired.

It has been shown that theory exists supporting the idea that the surface roughness of a sample can be obtained from the small-angle light back scattered (SALBS) pattern and that the surface character can be represented graphically by the Fourier transform of the SALBS pattern. It is also known that scattering is a conservative process and all light incident to the sample must be accounted for as either being absorbed, transmitted, scattered, or reflected. The part of the incident beam that is absorbed or transmitted is not a part of the SALBS pattern and can therefore be neglected in this treatment. The portion of the incident beam that is scattered by surface asperities is important for the graphical representation of the surface geometry but is not a part of the proposed method for surface roughness determination. The portion of the incident beam that composes the specular reflection is the basis for the proposed surface roughness determination method and the resultant roughness coefficient. The specular reflection was defined by Bennett and Porteus as

$$R_s = R_0 \exp\left[\frac{-(4\pi\sigma)^2}{\lambda^2}\right] \tag{6-1}$$

which can be rearranged to form an expression for a roughness coefficient

$$RC = \frac{R_s}{R_0} = \exp\left[\frac{-(4\pi\sigma)^2}{\lambda^2}\right] \tag{6-2}$$

The above equation proposed by Bennett and Porteus for the specular reflection, and the resultant roughness coefficient, does not appear to be related to equation 5-1 which fits the data obtained in this work. However, if the data is plotted as in Figure 6-1 with RC versus the rms squared roughness squared (σ^2) the following equation is obtained

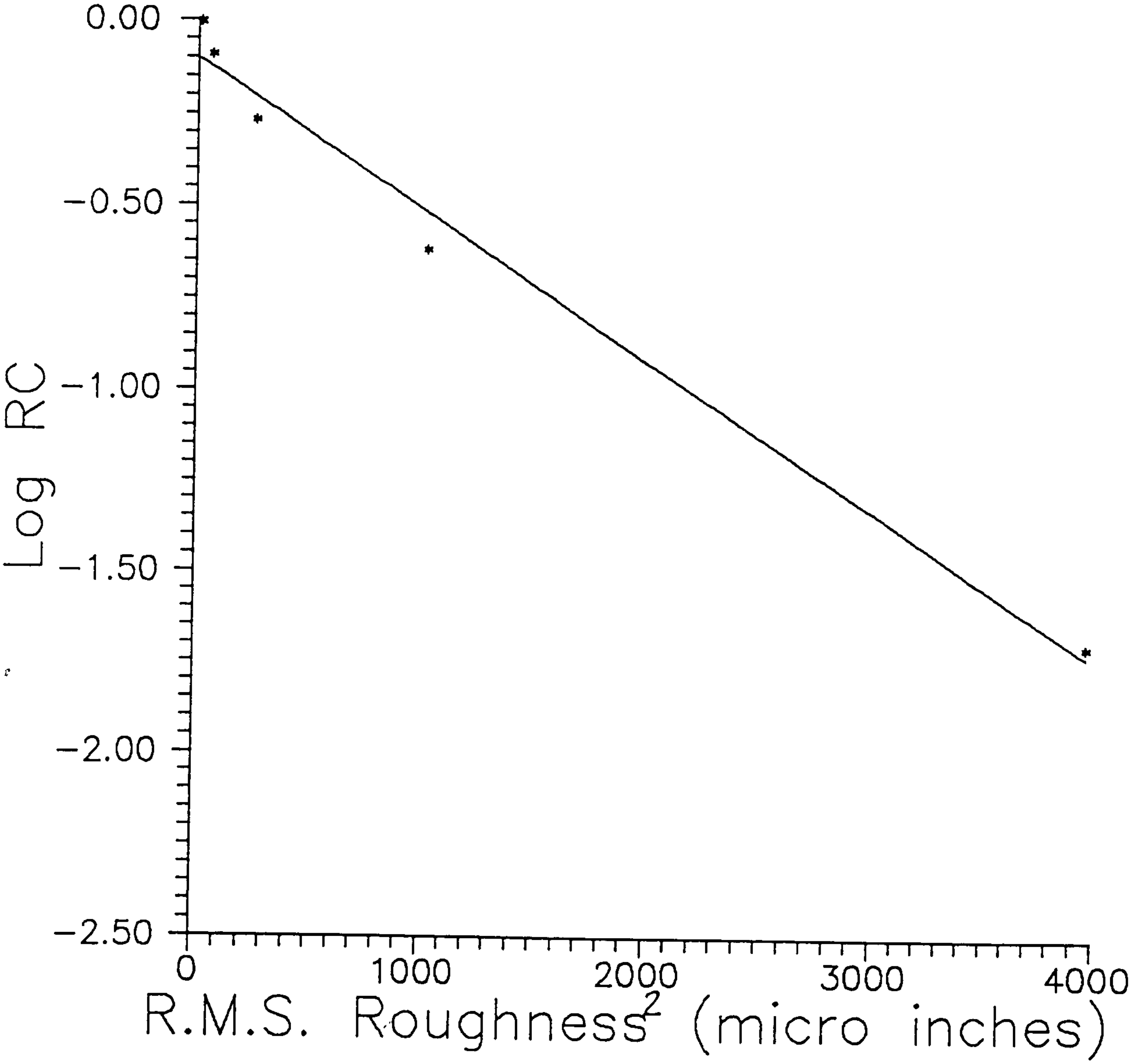

Figure 6.1 Log(RC) Versus RMS Roughness Squared

$$RC = C_1 \exp\left[\frac{-(C_2 4\pi\sigma)^2}{\lambda^2}\right] \tag{6-3}$$

Where C_1 and C_2 are calibration constants based on incident beam intensity, equipment geometry, camera f-stop, and camera contrast and gain settings. For this particular set of samples C_1 equals 0.89 and C_2 equals 0.1. It should be noted that this method is most applicable to systems where the samples have similar roughness characteristics or where the fibers are of similar diameters. In addition, this method is most applicable to the range of roughnesses greater than 1 microinch and less than 100 microinches. In order to obtain the root-mean-square roughness of a surface the equipment must be calibrated with a standard. If the equipment is not calibrated only relative roughness measurements are obtained. Although it is possible to obtain a greater degree of accuracy with other types of equipment, this method has certain advantages it is nondestructive, easy to operate, and relatively inexpensive. Additionally, it can easily be used for the rapid comparison of multiple samples.

The roughness coefficient gives a comparative value of the surface roughness, but does not reveal any details about the surface topography. Since the small-angle light back scattering pattern is in reciprocal space it was desirable to obtain a method of transforming the image to real space. With the use of an inverse Fourier transform defined as

$$f(x,y) = \sum_{u=0}^{M-1} \sum_{v=0}^{N-1} F(u,v) \exp\left[j2\pi\left(\frac{ux}{M} + \frac{vy}{N}\right)\right] \tag{6-4}$$

for x = 0,1,2,...,M-1, y = 0,1,2,...,N-1

it should be possible to obtain a graphical representation of the character of a sample's surface topography in real space. The representation will be similar to the one illustrated in Figure 6.2. The graphical representation of the surface topography should be used to support the calculated RC. The Fourier transformed images should be used to yield information on the orientation and distribution of the surface roughness present. The images obtained are the first known images to be numerically transformed from reciprocal space to real space. The images also show agreement with the type and magnitude of the known surface roughnesses represented on the surface roughness comparator. In addition the Fourier transformed fiber images show good agreement with the magnitude of the calculated roughness coefficient. However, it is not possible to evaluate the accuracy of the magnitude or character of the surface roughness values obtained for the fibers. This is due to the fact that neither the magnitude or character of the surface roughness has been obtained by other methods.

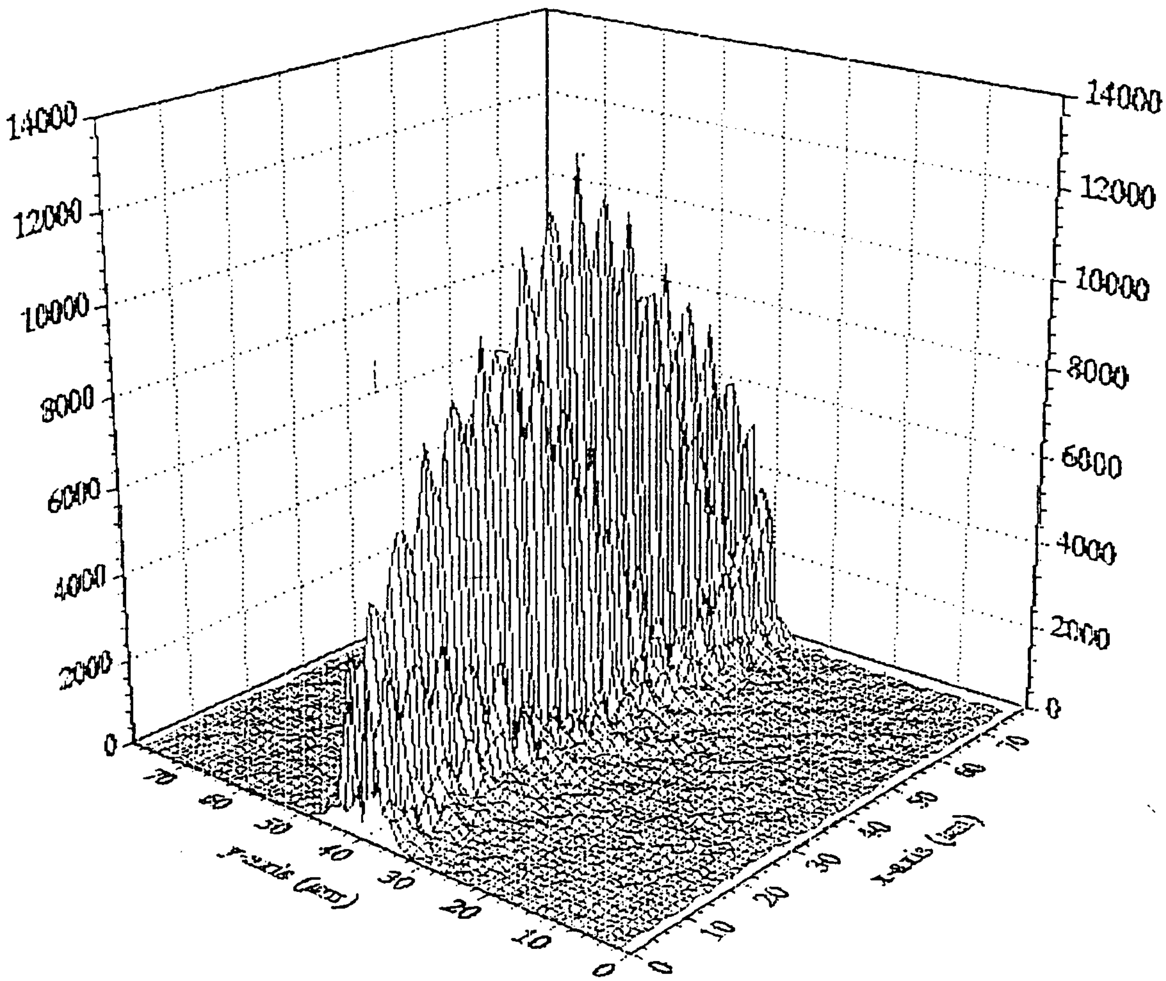

Figure 6.2 Typical Fourier Transformed Surface Roughness Pattern

VII. RECOMMENDATIONS

As Previously stated there are three areas where errors can enter into the procedures followed in this work. Theses areas include the contrast control on the camera, the model used to obtain the specular scattering, and the inconsistencies in intensity values caused by the first two problems. It is therefore recommended that a change be made in the equipment used to eliminate these problem areas. This change would be to use either a variable wavelength laser or two lasers of different wavelengths. The reasoning behind this can be understood by studying equation 2.1

$$R_s = R_0 \exp[-(4\pi\sigma)^2/\lambda^2]$$

If one plots Log $[R_s / R_o]$ versus σ^2, as in Figure 7.1, it can be seen that at increasing wavelengths as λ goes to and becomes greater than σ, Rc goes to 1 or in other words $R_s = R_o$.

With the availability of various wavelengths a wavelength could be chosen to cause the sample to appear smooth, the specular reflection could then be obtained directly. Also the specular pattern and the integrated pattern could be digitized within a short time frame. This would eliminate the need to adjust the camera's contrast between the two readings. It is probable that the intensity values recorded for two different wavelengths would not be directly comparable. However, it would

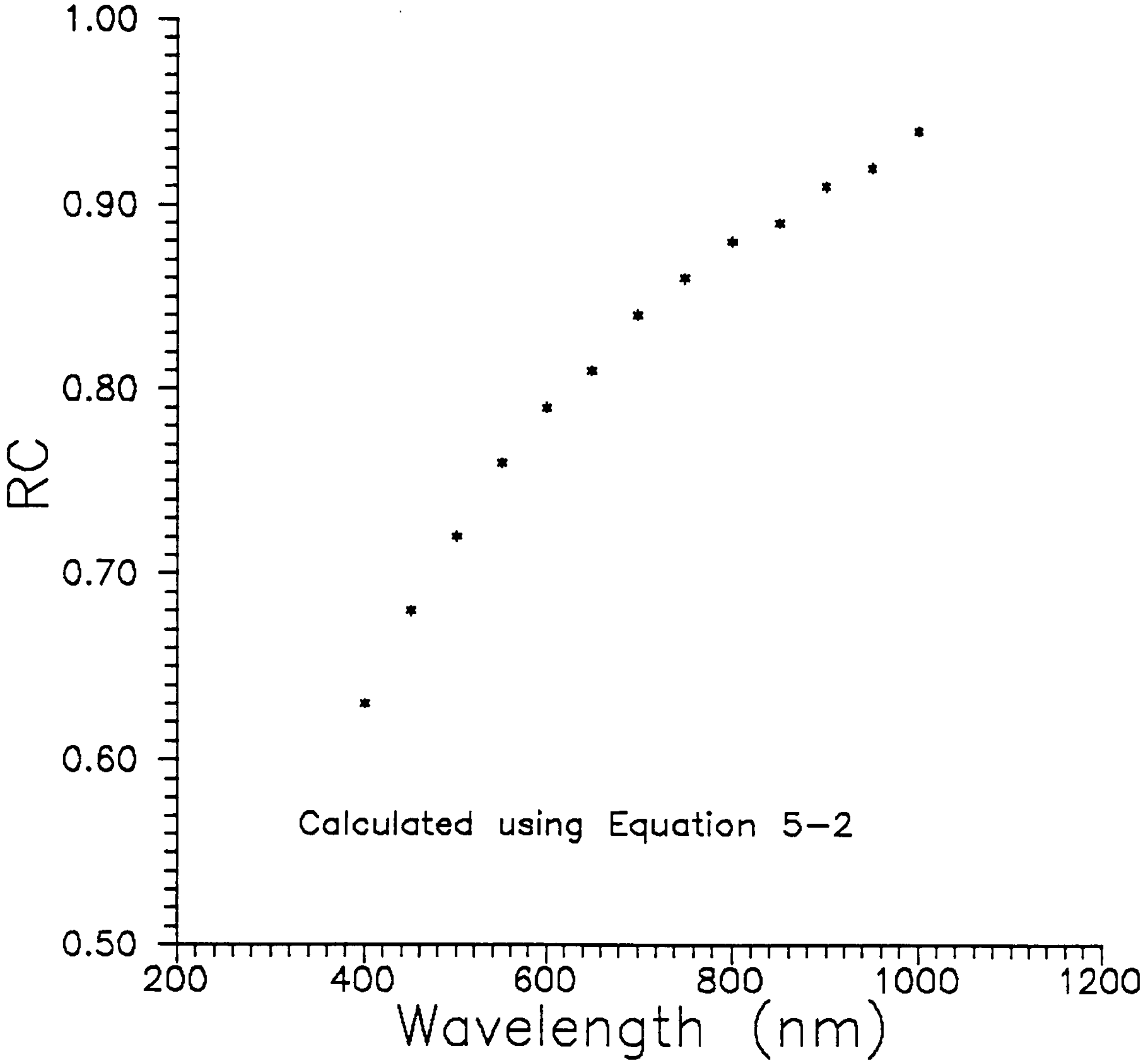

Figure 7.1 RC Versus Wavelength (8 microinch rms)

be a simple matter to correlate the intensity values from one wavelength to the other using a sample appearing smooth to both wavelengths. Using this method identical patterns should be obtained for both wavelengths.

In addition, when fiber samples, or samples with a smaller width than the diameter of the incident beam are used, several patterns should be recorded at each setting. Patterns should be recorded with the sample at various positions perpendicular to the incident beam; this should eliminate problems associated with the Gaussian characteristics of the beam.

In addition to eliminating errors in the experimental procedures it would be of interest to know how a wide variety of surface roughness types would affect the roughness coefficient and the Fourier transformed images. A set of experiments should be performed with samples of the same root-means-square roughness but with a variety of surface characteristics. This study would yield information on the use of the roughness coefficient to compare samples with varying types of roughness. In addition, the study would provide information on the use of Fourier transformed images to characterize surface roughness.

Bibliography

Bibliography

1. H.E. Bennett and J.O. Porteus, 'Relation Between Surface Roughness and Specular Reflectance at Normal Incidence', Journal of the Optical Society of America Vol. 51 No. 2, pp 123-129, (1961)

2. P. Beckmann, 'Scattering by Composite Rough Surfaces', Proceedings of the IEEE August 1965, pp 1012-1015

3. E.L. Church and J.M. Zavada, 'Residual Surface Roughness of Diamond-Turned Optics', Applied Optics Vol. 14 No. 8, pp 1788-1795, (1975)

4. P.J. Chandley, 'Determination of the Autocorrelation Function of Height on a Rough Surface from Coherent Light Scattering', Optical and Quantum Electronics 8(1976), pp 329-333

5. P.J. Chandley, 'Surface Roughness Measurements from Coherent Light Scattering', Optical and Quantum Electronics 8(1976), pp 323-327

6. J.M. Elson and J.M. Bennett, 'Relation Between the Angular Dependence of Scattering and the Statistical Properties of Optical Surfaces', J. Opt. Soc. Am. Vol 69 No. 1, pp 31-47, (1979)

7. E.C. Teague, T.V. Vorburger and D. Mayst'e, 'Light Scattering from Manufactured Surfaces', CIRP Vol. 30/2/1981

8. O.M. Mendez, A. Roger, and D. Maystre, 'Numerical Solution for an Inverse Scattering Problem of Non-Periodic Rough Surfaces', Appl. Phys. B 32, pp 199-206, (1983)

9. Y. Wang and W.L. Wolfe, 'Scattering from Microrough Surfaces: Comparison of Theory and Experiment', J. Opt. Soc. Am. Vol. 73 No. 11, pp 1596-1602, (1983)

10. D. Maystre, 'Rigorous Theory of Light Scattering from Rough Surfaces', J. Optics (Paris) Vol. 15 No. 1, pp 43-51, (1984)

11. E.L. Church, 'The Measurement of Surface Texture and Topography by Differential Light Scattering', Wear 57, pp 93-105, (1979)

12. C. Lou, 'Fiber Surface Characterization by Laser Back Scattering', Thesis, University of Tennessee, Knoxville, (1989)

13. R.A. Sprague, 'Surface Roughness Measurement Using White Light Speckle', Applied Optics Vol. 11 No. 12, pp 2811-2816, (1972)

14. B.J. Pernick, 'Surface Roughness Measurements with an Optical Fourier Spectrum Analyzer', Applied Optics Vol 18 No. 6, pp 796-801, (1979)

15. G.N. Clarke and T.R. Thomas, 'Roughness Measurement With a Laser Scanning Analyzer', Wear 57, pp 107-116, (1979)

16. E.G. Thwaite, 'The Direct Measurement of the Power Spectrum of Rough Surfaces by Optical Fourier Transformation', Wear 57, pp 71-80, (1979)

17. P.J. Chandley, 'Determination of the Probability Density Function of Height on a Rough Surface from Far-Field Coherent Light Scattering', Optical and Quantum Electronics 11, pp 412-418, (1979)

18. T. Horiuchi, Y. Tomita, and R. Kammel, 'Surface Roughness Measurement with Speckle Intensity Distribution Detected Using a Linear Image-Sensor', Japanese Journal of Applied Physics, Vol. 21, No. 12, pp L743-L745, (December 1982)

19 J.M. Bennett and L. Mattsson, 'Introduction to Surface Roughness and Scattering', (Optical Society of America, Washington, D.C.), (1989)

20 N.C. Geckinli and D. Yavuz, 'Discrete Fourier Transformation and Its Applications to Power Spectra Estimation', (Elsevier Scientific Publishing Company, New York), (1983)

21 H. Stark, 'Applications of Optical Fourier Transforms', (Academic Press, New York), (1982)

22 J.W. Goodman, 'Introduction to Fourier Optics', (McGraw-Hill Book Company, San Francisco), (1968)

23 L.J. Effler, Jr., 'Quantitative Small Angle Light Scattering of Liquid Crystalline Copolyester Films', Thesis, University of Tennessee, Knoxville, (1987)

24 M. Born and E. Wolf, 'Principles of Optics', (Pergamon Press, New York), (1964)

Appendixes

APPENDIX A

LISTING OF TSTREAK.BAS

```
10  REM * PROGRAM NAME:  TSTREAK.BAS
20  REM * PROGRAM AUTHOR:  THOMAS L. COX
30  REM * PROGRAM DATE:  20-APRIL-1990
40  REM * PROGRAM PURPOSE:  USING SNELL'S LAW AND THE
50  REM * INVERSE SQUARE LAW TO CREATE THE SMALL-ANGLE
60  REM * LIGHT REFRACTION FROM A PERFECTLY SMOOTH FIBER.
70  TOTINT = 0
80  CLS
90  INPUT "ENTER THE NAME FOR THE OUTPUT FILE "; N$
100 PRINT: PRINT
110 INPUT "ENTER THE SAMPLE-TO-SCREEN DISTANCE "; STS
120 PRINT: PRINT
130 INPUT "ENTER THE CAMERA-TO-SCREEN DISTANCE "; CTS
140 DIM N$(249)
150 OPEN N$ FOR OUTPUT AS #1
160 WRITE #1, 255
170 NORM = 1 / (STS)^2
180 X1 = 1 / (712.6 / (CTS)^1.05)
190 X = X1
200 FOR N = 2 TO 249
210 INTEN = 1 / ((STS)^2 + (X)^2)
220 X = X + X1
230 NORM1 = INT ((INTEN / NORM ) * 255)
240 WRITE # 1, NORM1
250 IF N >= 50 AND N <= 224 THEN TOTINT = TOTINT + NORM1
260 NEXT N
270 CLOSE #1
280 MULT = (905.9 / (CTS)^1.04) * .5
290 SUMINT = TOTINT * INT(MULT)
300 PRINT SUMINT
310 PRINT TOTINT
320 END
```

APPENDIX B

LISTING OF TDOT.BAS

```
10  REM * PROGRAM NAME:  TDOT.BAS
20  REM * PROGRAM AUTHOR:  THOMAS L. COX
30  REM * PROGRAM DATE:  20-APRIL-1990
40  REM * PROGRAM PURPOSE:  USING SNELL'S LAW AND THE
50  REM * INVERSE SQUARE LAW TO CREATE THE SMALL-ANGLE
55  REM * LIGHT REFRACTION FROM A PERFECTLY SMOOTH FLAT
60  REM * SAMPLE.
70  TOTINT = 0
80  CLS
90  INPUT "ENTER THE NAME FOR THE OUTPUT FILE "; N$
100 PRINT: PRINT
110 INPUT "ENTER THE SAMPLE-TO-SCREEN DISTANCE "; STS
120 PRINT: PRINT
130 INPUT "ENTER THE CAMERA-TO-SCREEN DISTANCE "; CTS
140 DIM N$(249)
150 OPEN N$ FOR OUTPUT AS #1
160 WRITE #1, 255
170 NORM = 1 / (STS)^2
180 X1 = 1 / (712.6 / (CTS)^1.05)
185 N1 = X1 * (0.5 / SIN(3.1416/2))
190 X = X1
200 FOR N = 1 TO N1
210 INTEN = 1 / ((STS)^2 + (X)^2)
220 X = X + X1
230 NORM1 = INT ((INTEN / NORM ) * 255)
240 WRITE # 1, NORM1
250 IF N >= 50 AND N <= 224 THEN TOTINT = TOTINT + NORM1
260 NEXT N
270 CLOSE #1
280 MULT = (905.9 / (CTS)^1.04) * .5
290 SUMINT = TOTINT * INT(MULT)
300 PRINT SUMINT
310 PRINT TOTINT
320 END
```

APPENDIX C

LISTING OF 2DFFT.FOR

```
C     The program 2DFFT.FOR was written by ESB on 7/8/91
C     2DFFT.FOR performs a 2-D fast Fourier Transform on a
C     data file and places the output into another file.  The
C     program is based on FFT subroutine given by Brigham in
C     "The Fast Fourier Transform".
C
      INTEGER N,NU,X,Y,Z,G,H,I,J,IEXPORT(256)
      INTEGER CENTER,SIGNN,FORMAT
      REAL*4 XREAL(256),XIMAG(256),YREAL(128),YIMAG(128),XMAG
      REAL*4 A(256,128),B(256,128),REXPORT(256),IA,IMAX
      CHARACTER*12 INPUT, OUTPUT
      COMMON REALD,IMAGD,A,B
20    FORMAT(I9,256I10)
30    FORMAT(I9,256E10.4)
C
C     ACQUIRE INITIAL STARTUP DATA
C
      CALL QUESTION(INPUT,OUTPUT,CENTER,SIGNN,FORMAT)
      OPEN (3,FILE=INPUT,STATUS='OLD')
      READ(3,*) Y,X,Z
C
C     READ IN DATA FROM INPUT FILE
C
      WRITE(*,*) '        READING DATA'
      WRITE(*,*) ' '
      DO 50 J = 1, Y
            DO 40 I = 1, X
                  READ(3,*) G,H,IA
                  IF (CENTER .EQ. -1) THEN
                        IA=IA*(-1)**(I+J)
                  END IF
                  A(I,J)=IA
40          CONTINUE
50    CONTINUE
      CLOSE(3)
C
C     PERFORM ROW TRANSFORM
C
      WRITE(*,*) '        CALCULATING TRANSFORM'
      WRITE(*,*) ' '
      N=X
      NU=INT(LOG(X)/LOG(2))
      DO 80 J = 1, Y
            DO 60 I = 1, X
                  XREAL(I)=A(I,J)
60          CONTINUE
            CALL FFTS(N,NU,XREAL,XIMAG,SIGNN)
            DO 70 I = 1, X
                  IF (SIGNN .EQ. 1) THEN
                        A(I,J) = XREAL(I)*Y/X
                        B(I,J) = XIMAG(I)*Y/X
                  ELSE
```

```
                  A(I,J) = XREAL(I)
                  B(I,J) = XIMAG(I)
            END IF
            XIMAG(I) = 0
70       CONTINUE
80    CONTINUE
C
C     PERFORM COLUMN TRANSFORM
C
      N=Y
      NU=INT(LOG(Y)/LOG(2))
      DO 110 I = 1, X
         DO 90 J = 1, Y
            YREAL(J)=A(I,J)
            YIMAG(J)=B(I,J)
90       CONTINUE
         CALL FFTS(N,NU,YREAL,YIMAG,SIGNN)
         DO 100 J = 1, Y
            IF (SIGNN .EQ. 1) THEN
                  A(I,J) = YREAL(J)/Y
                  B(I,J) = YIMAG(J)/Y
            ELSE
                  A(I,J) = YREAL(J)
                  B(I,J) = YIMAG(J)
            END IF
100      CONTINUE
110   CONTINUE
C
C     WRITE DATA TO OUTPUT FILE
C
      WRITE(*,*) '         WRITING DATA TO OUTPUT FILE'
      WRITE(*,*) ' '
      OPEN(4,FILE=OUTPUT,STATUS='UNKNOWN')
      IF (FORMAT .EQ. -1) GOTO 150
      WRITE(4,*) Y+1, X+1
      J=0
      DO 120 I = 1, X
         IEXPORT(I) = I
120   CONTINUE
      WRITE(4,20) J, IEXPORT
      DO 140 J = 1, Y
         DO 130 I = 1, X
            XMAG = SQRT(A(I,J)**2+B(I,J)**2)
            REXPORT(I)=XMAG
            IMAX = MAX(IMAX,XMAG)
130      CONTINUE
         WRITE(4,30) J, REXPORT
140   CONTINUE
      GOTO 180
150   WRITE(4,*) Y,X,Z
      DO 170 J = 1, Y
         DO 160 I = 1, X
```

```
                  XMAG = SQRT(A(I,J)**2+B(I,J)**2)
                  IMAX = MAX(IMAX,XMAG)
                  WRITE(4,*) J,I,XMAG
160           CONTINUE
170      CONTINUE
180      CLOSE(4)
         WRITE(*,190) IMAX
190      FORMAT(1X,'The maximum value of the transform is ',F10.2)
         END

         SUBROUTINE FFTS(N,NU,XREAL,XIMAG,F)
         INTEGER K,K1,K1N2,I,N,N2,NU,NU1,P,F
         REAL*4 ARG,C,S,TREAL,TIMAG,XREAL(512),XIMAG(512)
         N2=N/2
         NU1=NU-1
         K=0
         DO 30, L=1,NU
10            DO 20, I=1,N2
                  P=IBITR(K/2**NU1,NU)
                  ARG=6.283185*REAL(P)/REAL(N)
                  C=COS(ARG)
                  S=SIN(ARG)*F
                  K1=K+1
                  K1N2=K1+N2
                  TREAL=XREAL(K1N2)*C+XIMAG(K1N2)*S
                  TIMAG=XIMAG(K1N2)*C-XREAL(K1N2)*S
                  XREAL(K1N2)=XREAL(K1)-TREAL
                  XIMAG(K1N2)=XIMAG(K1)-TIMAG
                  XREAL(K1)=XREAL(K1)+TREAL
                  XIMAG(K1)=XIMAG(K1)+TIMAG
                  K=K+1
20            CONTINUE
              K=K+N2
              IF(K.LT.N) GOTO 10
              K=0
              NU1=NU1-1
              N2=N2/2
30       CONTINUE
         DO 40 K=1,N
              I=IBITR(K-1,NU)+1
              IF (I.LE.K) GOTO 40
              TREAL=XREAL(K)
              TIMAG=XIMAG(K)
              XREAL(K)=XREAL(I)
              XIMAG(K)=XIMAG(I)
              XREAL(I)=TREAL
              XIMAG(I)=TIMAG
40       CONTINUE
         RETURN
         END

         FUNCTION IBITR(J,NU)
```

```
      INTEGER NU,IBITR,J,J1,J2
      J1=J
      IBITR=0
      DO 10 I=1,NU
            J2=J1/2
            IBITR=IBITR*2+(J1-2*J2)
            J1=J2
10    CONTINUE
      RETURN
      END

      SUBROUTINE QUESTION(INPUT,OUTPUT,CENTER,SIGNN,FORMAT)
      INTEGER CENTER,SIGNN,FORMAT,KEY,WAITKY
      CHARACTER*12 INPUT,OUTPUT
      WRITE(*,*) ' '
      WRITE(*,*) 'Enter the name of the input file with ext. [.DAT].'
      READ(*,10) INPUT
10    FORMAT (A12)
      WRITE(*,*) ' '
      WRITE(*,*) 'Enter the name of the output file with ext. [.DAT].'
      READ(*,10) OUTPUT
      WRITE(*,*) ' '
      WRITE(*,*) 'Do you want a forward or reverse transform, [F,R]?'
20    KEY = WAITKY()
      IF (KEY .EQ. 70 .OR. KEY .EQ. 102) THEN
            SIGNN = 1
            WRITE(*,*) 'Forward Transform'
      ELSE IF (KEY .EQ. 82 .OR. KEY .EQ. 114) THEN
            SIGNN = -1
            WRITE(*,*) 'Reverse Transform'
      ELSE
            GOTO 20
      END IF
      WRITE(*,*) ' '
      WRITE(*,*) 'Do you want a centered transform, yes or no [Y,N]?'
30    KEY = WAITKY()
      IF (KEY .EQ. 89 .OR. KEY .EQ. 121) THEN
            CENTER = -1
            WRITE(*,*) 'Centered Transform'
      ELSE IF (KEY .EQ. 78 .OR. KEY .EQ. 110) THEN
            CENTER = 1
            WRITE(*,*) 'Plain Transform'
      ELSE
            GOTO 30
      END IF
      WRITE(*,*) ' '
      WRITE(*,*) 'Do you want the output in a column or grid file format
     1 [C,G]?'
40    KEY = WAITKY()
      IF (KEY .EQ. 67 .OR. KEY .EQ. 99) THEN
            FORMAT = -1
            WRITE(*,*) 'Column format'
```

```
ELSE IF (KEY .EQ. 71 .OR. KEY .EQ. 103) THEN
      FORMAT = 1
      WRITE(*,*) 'Grid format'
ELSE
      GOTO 40
END IF
WRITE(*,*) ' '
END
```

APPENDIX D

LISTING OF RC.FOR

```
C        PROGRAM NAME:  RC.FOR
C        PROGRAM AUTHOR:  THOMAS LEVITTE COX
C        PROGRAM PURPOSE: TO SUM THE INTENSITY VALUES WITH
C        THE GIVEN RANGE, AND DETERMINE THE SURFACE
C            ROUGHNESS COEFFICIENT
        CHARACTER FNAME*12
        INTEGER XSTRT, YSTRT, XSTOP, YSTOP, ER, ER1, TINTEN
        INTEGER INTEN, TINT
        INTEGER X, Y
        REAL RC
        TINTEN = 0
        WRITE (*,*) 'ENTER THE FILENAME'
        READ (*,*) FNAME
        CALL GETDAT(FNAME,ER)
        WRITE (*,*) 'ENTER THE THEORITICAL INTENSITY TOTAL'
        READ (*,*) TINT
        WRITE (*,*) 'ENTER THE STARTING X-COORDINATE'
        READ (*,*) XSTRT
        WRITE (*,*) 'ENTER THE STARTING Y-COORDINATE'
        READ (*,*) YSTRT
        WRITE (*,*) 'ENTER THE ENDING X-COORDINATE'
        READ (*,*) XSTOP
        WRITE (*,*) 'ENTER THE ENDING Y-COORDINATE'
        READ (*,*) YSTOP
        DO Y = YSTRT, YSTOP
               DO X = XSTRT, XSTOP
               CALL GETPNT(X,Y,INTEN,ER1)
               TINTEN = TINTEN + INTEN
               ENDDO
        ENDDO
        WRITE (*,100) ' TOTAL INTENSITY' , TINTEN
100     FORMAT(A16, 5X, I7)
        RC = REAL(TINTEN) / REAL(TINT)
        WRITE (*,200) ' RC', RC
200     FORMAT(A3, 5X, F5.3)
        END
```

VITA

Thomas Levitte Cox was born October 28, 1964. He grew up in the town of Rockwood, Tennessee where he completed his elementary education and graduated from Rockwood High School in June of 1982. He received his Bachelor of Science Degree in Chemical Engineering in June 1986, from the University of Tennessee, Knoxville. Upon graduation he entered the graduate program at the University of Tennessee while working part time at the Oak Ridge National Laboratory for the Graduate Program in Library Science.